deutschen

SHOCK WAVES IN NUCLEAR MATTER - PROOF BY CIRCUMSTANTIAL EVIDENCE

Inaugural - Dissertation
zur
Erlangung des Doktorgrades der Naturwissenschften
vorgelegt beim Fachbereich Physik der
Johann Wolfgang Goethe - Universität
zu Frankfurt am Main

von

Horst Stöcker
aus
Frankfurt am Main

Frankfurt am Main
1979

— Physik

Dekan: Prof. Dr. Marteussen

1. Gutachter: Prof. Dr. Greuer

2. Gutachter: Prof. Dr. Schopper

Tag der mündl. Prüfung:

Tag der Promotion: 2.11.1979

Shock Waves in Nuclear Matter - Proof by Circumstantial Evidence[1]

H. STÖCKER, J. HOFMANN, J. A. MARUHN, and W.GREINER[2]

Institut für Theoretische Physik der Johann Wolfgang, Goethe-Universität, Frankfurt am Main, West Germany

ABSTRACT

In the present paper we develop the essential theoretical tools for the treatment of the dynamics of High Energy Heavy Ion Collisions. We study the influence of the nuclear equation of state and discuss the new phenomena connected with phase transitions in nuclear matter (pion condensation). Furthermore we investigate the possibility of a transition from nuclear to quark matter in High Energy Heavy Ion Collisions. In this context we discuss exotic phenomena like strongly bound pionic states, limiting temperatures, and exotic nuclei.

KEYWORDS

High Energy Heavy Ion Collisions, compression, shock waves, nuclear fluid dynamics, pion condensation, density isomers, quark matter.

1. INTRODUCTION

One of the most exciting motivations for the high energy heavy ion physicist is the possibility to study the nuclear equation of state at high densities, temperatures and pressures (Scheid, 1968; Chapline, 1973; Scheid, 1974; Scheid, 1974a; Wong,1974; Heinz, 1978), as well as the search for phase transitions into abnormal superdense states of matter like pion condensates (Migdal, 1972; Brown, 1975; Brown, 1976; Migdal, 1978; Campbell, 1975), density isomers (Lee, 1974), and quark matter (Collins, 1975; Baym, 1976; Keister, 1976).

We will concentrate on the following topics:

First we discuss the semi-validity of the nuclear fluid dynamical model which we use later on to describe high energy nuclear collisions. Then the nuclear equation of state is discussed, together with the compressibility, phase transitions like pion condensates and density isomers and the baryon-quark matter.

---

[1] Supported by Bundesministerium für Forschung und Technologie (BMFT), and by the Gesellschaft für Schwerionenforschung (GSI).

[2] Invited speaker at the Erice School on Heavy Ion Interactions at High Energies, Erice (Italy), 26 March - 6 April, 1979.

By comparing the results of the hydrodynamical approach with a number of recent experiments we will discuss the circumstantial evidence for the occurrence of strong compression effects (shock waves) and high thermal excitation. Finally we speculate about the phenomena which may occur at very high energies.

2. APPLICABILITY OF THE HYDRODYNAMICAL APPROACH

For the applicability of the fluid dynamical concepts it has to be ensured that fast equilibration and thermalization of the incident momentum and energy occurs in high energy heavy ion collisions, and that the mean free path (more precisely: the longitudinal momentum decay length) over the typical dimension, L, of the system is small $\lambda/L << 1$.
The mean free path λ is given by

$$\lambda = \frac{1}{\sigma \cdot \rho}$$

where σ is the total nucleon-nucleon scattering cross section and ρ is the actual nuclear density. For normal nuclear density ρ_o and a free n-n scattering cross section $\sigma_{NN} \sim 30$ mb at high energies, the mean free path is $\lambda \sim 2$fm, which is not too small against the nuclear dimensions L~10fm (Scheid,1968; 1974; 1974a).

High relative momenta between nuclei, signifying no overlap in phase space, as well as the large longitudinal momentum decay length calculated from the free n-n scattering cross section were interpreted as a complete transparency for the two nuclei at high energies and as a death for compression (shock) waves at energies above 1 GeV/n (Sobel,1975). However, in the "formation flight" of ensembles of nucleons, collective scattering phenomena (Gyulassy,1977; Ruck,1976) and compression effects can not be neglected, so that the scattering cross section and the density can be modified drastically leading to a decrease of the mean free path

$$\lambda \simeq 1.4 \frac{\sigma_{NN}}{\sigma_{coll}} \cdot \frac{\rho_o}{\rho} \text{ fm} \quad .$$

Pions and pionic waves produced in inelastic nucleon collisions via the creation and decay of nuclear isobars (Hofmann,1976) (nucleon resonances) in processes of the type

$$N + N \rightarrow N + N^* \rightarrow N + \pi + N \rightarrow N^* + N \rightarrow \ \ldots$$

and via pionic bremsstrahlung (Vasak,1979) may lead to rapid randomization of longitudinal momentum and energy, and thus to a short mean free path and to generation of shock waves.

Another important process for randomization is the critical scattering of nucleons in the vicinity of a phase transition point (Gyulassy,1977). This is in analogy to the critical opalescence, which is characterized by the great enhancement of the scattering cross section of light near a liquid-gas phase transition, or of the critical scattering of neutrons in ferromagnets near the Curie point (Stanley, 1971) or - as the last example - the critical scattering appearing in two colliding plasma beams: When the drift velocity of the two plasmas exceeds a critical value, unstable plasmon modes appear, resulting in a growth of strong electric fields, which greatly reduce the penetration depth of the two plasmon beams in comparison to values estimated from free two-body collisions.

Thus, the vicinity of a phase transition - e.g. the onset of pion condenstion or gluon condensation is expected to be marked by the occurrence of critical nucleon-nucleon scattering, i.e. a large enhancement (a factor of 2-4 for pion condensation) of the density-dependent n-n cross section (Gyulassy,1977; Ruck,1976).

Together with the doubling of the nuclear density due to the overlap of nuclear matter the mean free path can then reduce by a factor of 4-8 or more to

$$\lambda \lesssim 0.4 \text{ fm}$$

This would mean that even at bombarding energies above one GeV/n nuclei do not become transparent to each other: On the contrary,very violent collisions can be expected. One should keep in mind, however, that nucleus-nucleus collisions are a quantum meachanical process.Hence - in the sense of quantum mechanical fluctuations - under the same initial conditions processes with violent randomization (i.e. the occurrence of pronounced shock waves) may occur as well as processes with less pronounced interaction. It is a formidable experimental task to separate the former from the latter.

Indeed, recent experiments (which we discuss later) show that up to lab-energies of 4 GeV/n a considerable part ($\sim$ 30%) of the total cross section are violent events with high multiplicities and large momentum transfer.

3. THE EQUATION OF MOTION

The most complete representation of nuclear hydrodynamics is given for the non-relativistic case by the Navier-Stokes equations, where the nuclear viscosity and thermal conductivity are included as well as a realistic treatment of the nuclear binding and surface via the Coulomb- and Yukawa potential (Wong,1977; Maruhn,1977; Stöcker,1979). The equations of motion express the conservation of particle number

$$\frac{\partial \rho}{\partial t} + \nabla \cdot (\rho \vec{v}) = 0 \tag{1}$$

momentum

$$\frac{\partial (\rho m v)}{\partial t} + \nabla (m \rho \vec{v} \cdot \vec{v}) = -\nabla \vec{S} - \rho \nabla V \tag{2}$$

and - energy

$$\frac{\partial (\rho E)}{\partial t} + \nabla (\rho E v) = \nabla (\kappa \nabla T) - \nabla (\overleftrightarrow{S} \cdot \vec{v}) - \rho v \cdot \nabla V \tag{3}$$

where $\overleftrightarrow{S}$ a Newtonian form has been assumed. The potential, which allows a realistic treatment of the nuclear binding and surface is a sum of the Coulomb potential determined via the Poisson-equation

$$\nabla^2 V_c(\vec{r}) = -4\pi \left(\frac{Ze}{A}\right)^2 \rho(\vec{r}) \tag{4}$$

and a Yukawa potential V_y given by

$$(\nabla^2 - \alpha^2) V_y(\vec{r}) = -4\pi\beta \rho(\vec{r}) \quad . \tag{5}$$

The Yukawa force allows for a smoothed nuclear surface - a realistic surface thickness can be obtained e.g. with the parameters $\alpha = 2.1 \text{ fm}^{-1}$ and $\beta = -280$ MeV fm corresponding to a nuclear surface energy coefficient

$$\eta = 2\pi \frac{\beta}{\alpha^4} \sim 90 \text{ MeV fm}^5 \tag{6}$$

Up to now, three-dimensional nuclear fluid dynamical calculations have only been performed using the Euler equations, i.e. the equations of motion for an ideal - i.e. non-viscous and non-thermo-conducting fluid (eq. (1),(2),(3) with η, K=0).

(Stöcker,1979). The above equations describe fluid dynamical processes completely. However, it is often advantageous to gain more insight into the physical processes by solving more simplified, schematic models, which can be solved (at least to some extent) analytically. In this case another set of equations is applied in the more schematic treatment of the fluid-dynamical description of high energy heavy ion collisions, namely the shock equations:

Shock waves have to be clearly distinguished from sound waves. In contrast to sound waves, shock waves are connected with a strong, density dependent mass flow with a flow velocity v_f. The shock front itself propagates with the shock velocity $v_s > v_f$ and does also depend strongly on the compression amplitude (Baumgardt,1975). Shock waves are non-linear phenomena - for large amplitudes $\rho \gg \rho_o$ both v_s and v_f tend to the velocity of light (see Fig. 1), while for small perturbations $\rho \sim \rho_o$ they approach the linear limit of sound waves. Shock waves imply a large entropy production: The matter flow through the shock front is highly irreversible, it is not only connected with strong compression, but also with large thermal excitation (Hofmann,1976; Stöcker,1977,1977a,1978).

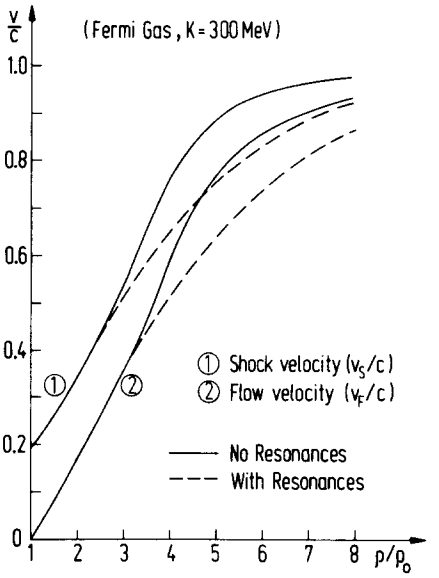

Fig. 1. shows the strong dependence of the shock velocity v_s and the flow velocity of v_f on the compression.

The shock calculations have to be viewed as an idealization assuming a zero width of the shock front together with the discontinuous jump of the state variables(e.g. ρ,T,e,p). However, the comparison of the nuclear shock wave calculations with the result of the full Navier Stokes calculations (Stöcker,1979b) show that the resulting compression rates and temperatures are very similar, although in the Navier Stokes calculations the compression front is smeared out over 1-2 fm due to the viscosity. Such a width seems to be rather realistic, as the width of a shock front is approximately given by 2-3 mean free path, which can be less than half a fermi in high energy nuclear collisions. For a large nuclear transparency, the shock front width may be of the order of the nuclear radius. However, no indication for transparency has been found in the high energy experiments up to now.

The relativistic shock equations (Baumgardt,1975) can be derived from the continuity of the

$$\begin{aligned} &\text{particle flux density} && [j^o] = [\rho\, u_x] = 0 \\ &\text{energy flux density} && [T_{ox}] = [i\, u_o u_x] = 0 \\ &\text{and momentum flux density} && [T_{xx}] = [i\, u_x^2 + p] = 0 \end{aligned} \tag{7}$$

where [ ] denotes the jump of the respective variable across the shock front, and x gives the direction normal to the shock front as seen from the shock front's rest frame.

Eliminating the velocities u_x from the continuity equations yields the relativistic shock equation

$$\frac{i_o^2}{\rho_o^2} - \frac{i^2}{\rho^2} + (p-p_o)\left(\frac{i_o}{\rho_o^2} - \frac{i}{\rho^2}\right) = 0 \tag{8}$$

which gives an unique connection between the free enthalpy i, pressure p, and density ρ within the respective rest frame of the matter (subscript o stands for the undisturbed matter in front of the shock wave, quantities without subscript refer to matter in the compressed state). When we insert $i = \rho W + p$ and $i_o = \rho_o W_o$ the equation

$$W^2 - W_o^2 + p\left(\frac{W}{\rho} - \frac{W_o}{\rho_o}\right) = 0 \tag{9}$$

is obtained. Here $W(\rho,T)$ is the energy density functional, which characterizes the nuclear equation of state. It will be discussed in the next section. Neglecting pions and resonances and regarding the pure nucleon fluid only, the relation $p_T = \alpha\rho\, E_T$ obtained in the next section can be used to obtain a quadratic equation in E_T, which can be solved in terms of the nucleon density ρ analytically. E_T is the temperature-dependent part of $W(\rho,T)$.

For the non-relativistic case $\alpha = \frac{2}{3}$, the temperature is easily calculated from E_T:

$$T = \left(\frac{2\, E_T\, \rho^{2/3}}{\beta}\right)^{1/2} . \tag{10}$$

It is important to note that the thermal energy of the nucleon gas does not depend on the gas ansatz for E_T, but only on the relation $p_T = 2/3\, \rho\, E_T$. Thus this equation is also valid for a classical ideal gas, whereas the temperature in the compressed matter depends drastically on the gas ansatz $T = \frac{2}{3} E_T$ for the classical gas. (see Fig. 2).

The inclusion of pions and resonances demands for an numerical iterative solution of the shock equation,as the pressure is now more complicated.

The shock velocities v_s and v_f can be determined by the continuity of the energy and momentum flux density. From the relative velocities of the matter with respect to the shock front, the relative matter flow velocity v_f is obtained by covariant summation (see Figs. 1 and 3).

$$\begin{aligned} \frac{v_s}{c} &= \left\{ \frac{p\, w\, \rho}{(w_\rho - w_o\rho_o)(w_o\rho_o + p)} \right\}^{1/2} \\ \frac{v_f}{c} &= \left\{ \frac{p(\rho w - \rho_o w_o)}{\rho w\, (p + \rho_o w_o)} \right\}^{1/2} \end{aligned} \tag{11}$$

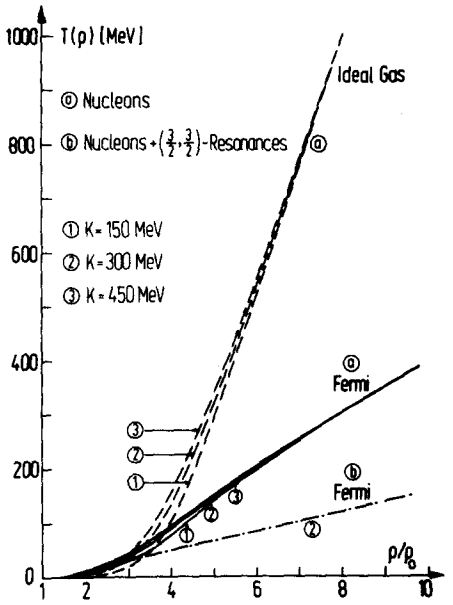

Fig. 2. The density dependence of the temperature T is shown for different equations of state and compression constants K.

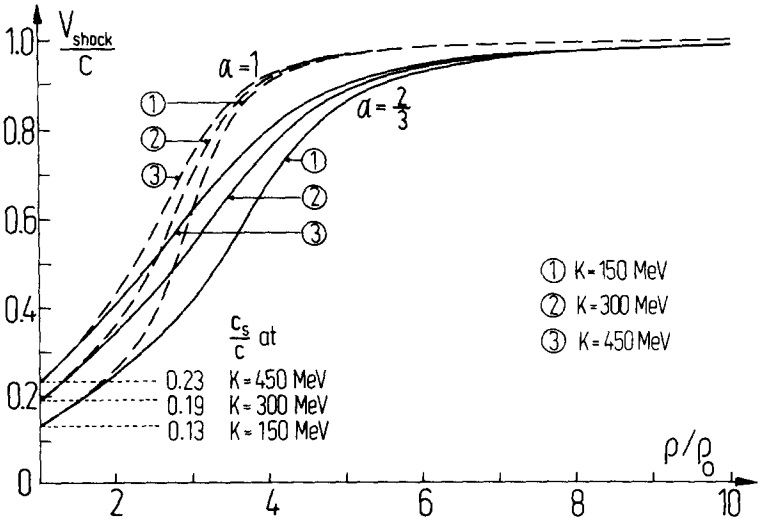

Fig. 3. The dependence of the shock velocity on the compression constant is shown.

A one dimensional relativistic shock model

A simple illustration model can be constructed to calculate the shock compression and -temperature in the central collision of two heavy nuclei as a function of the bombarding energy (Baumgardt,1975; Stöcker,1978). This model assumes the compressed fluid to be at rest in the center-of-momentum system (equal velocity frame). Three-dimensional fluid dynamical calculations show that this requirement is fulfilled fairly well for non-peripheral collisions of heavy nuclei near the collision axis: A sort of stationary compression stage develops. That means, that practically all of the incident kinetic energy is transformed into internal energy (compression and excitation).

As v_f denotes the relative velocity from the laboratory to the shocked matter in the c-M frame, the lab energy is given by

$$E_{LAB} = \left[\left(1 - \left(\frac{v_p}{c}\right)^2\right)^{-1/2} - 1 \right] W_o \qquad (12)$$

where $v_f = \frac{2v_f}{1+(v_{f/c})^2}$ denotes the projectile velocity.

Though this model will, due to the lack of kinetic energy of the compressed matter and due to the outflow of matter perpendicular to the collision axis (as compared to three dimensional calculations), give too large values for compression and temperatures as function of the bombarding energy, it is sufficiently good to give a rather quantitative overview about the expected compression and thermal excitation. The influence of the beam energy and the nuclear equation of state (e.g. different compressibility constants) and the importance of resonance and pion production on the collision dynamics can be studied rather nicely at very low cost - the integration of the full three dimensional fluid model actually is not yet possible with the inclusion of resonances. The results of this model calculations are presented in section 7.

4. THE NUCLEAR EQUATION OF STATE

Usually one starts with the energy per nucleon $W(\rho,T)$ for which we use the ansatz

$$W(\rho,T) = M_o c^2 + E_c(\rho) + E_T(\rho,T) \qquad (1)$$

for purely nucleonic fluid. Here $M_o c^2$ is the nucleon's rest energy, $E_c(\rho,T=0)$ phenomenologically reflects the nuclear binding energy, the Fermi energy, the hard (soft) core and the exchange parts of the nuclear forces. For $E_c(\rho)$ one usually uses a power expansion in the density as obtained in nuclear matter calculations. We will use a parabolic expansion known from the extended liquid drop model (Scheid, 1969)

$$E_c(\rho) = \frac{K_o}{18\,\rho\rho_o}(\rho - \rho_o)^2 + B_o \qquad (2)$$

where $B_o = -16$ MeV and $K_o = 200$ MeV is the nuclear compression constant.

Secondary minima (density isomers) are represented by a similar ansatz with different ρ_1, K_1, B_1. For the thermal energy, the simplest ansatz is the classical ideal gas $E_T = 3/2\ T$. (See Fig. 4).

We will also use the Fermigas expansion

$$E_T(\rho,T) = \frac{\beta}{2}\rho^{-2/3}T^2 = \frac{\sigma^2}{2\beta}\rho^{2/3} = E_T(\rho,\sigma) \qquad (3)$$

where we used the standard thermodynamical relations

$$T = \frac{\partial W}{\partial \sigma}\Big|_{\rho} = \frac{\sigma}{\beta}\ \rho^{2/3} \quad , \quad \beta = \left(\frac{g\pi}{6}\right)^{2/3}\ \frac{mc^2}{(\hbar c)} \quad , \tag{4}$$

σ being the nucleon's specific entropy.

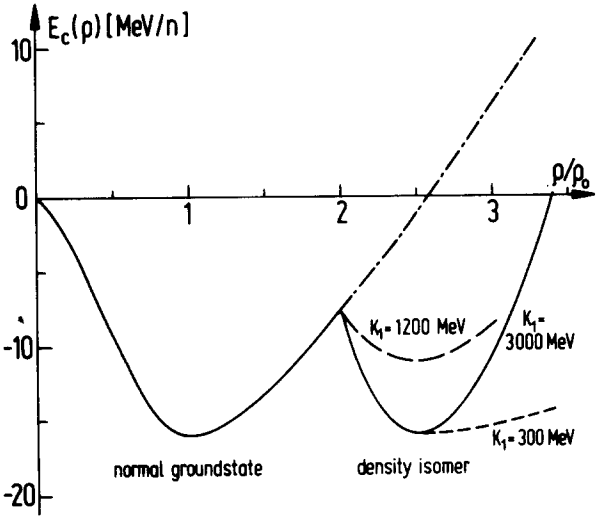

Fig. 4. The compression energy with the various possibilities for a density isomer is shown.

At high temperatures, the production of resonances becomes important (Hofmann,1976) The resonance excitation is treated thermodynamically, where the following approximations have been used. As practically nothing is known about the nucleon - N^* and N^* - N^* interactions, we assume that the N^* interaction does also only depend on the total baryon density. Therefore the compression energy $E_c(\rho)$ is unchanged, ρ being now the baryon number density. The first difference is the thermal excitation energy of the isobars. Using the free Fermi gas expansion as above the thermal energy of a resonance with mass $m_i c^2$ is given by

$$E_{T_i} = \frac{1}{2}\,\beta_i\ \rho_i^{-2/3}\ T^2 \tag{5}$$

where

$$\beta_i = (\tau_i/6^{\pi})^{2/3}\ \frac{m_i c^2}{\hbar c}$$

and ρ_i is the density of the i-th resonance phase.

The resonances can be viewed as excited nucleons (resonance pair production is not important at the above temperatures). A Boltzmann distribution for the excitation probability of the i-th resonance has been assumed. Ensuring baryon number conservation, one obtains the partitions

$$\lambda_i = \frac{\tau_i\ e^{E_{i/T}}}{\Sigma\ \tau_k\ e^{-E_k/T}} \tag{6}$$

where $$\tau_i = \frac{g_i}{g_n} = \frac{(2\ \text{Spin (i)} + 1) \cdot (2\ \text{Isospin (i)} + 1)}{4}$$

is the statistical weight factor of the i-th resonance, and $E_i = (m_i - m_o)\, c^2$ is the energy necessary for the resonance excitation.

The density of the i-th phase is then given by

$$\rho_i = \lambda_i\, \rho \tag{7}$$

and the total energy density $e = \rho W$ is given as the sum over the energy densities of all phases

$$e = \sum_i e_i = \sum_i \rho_i\, W_i. \tag{8}$$

As all baryons are assumed to interact only via $E_c(\rho)$, the energy per resonance i is

$$W_i = m_i\, c^2 + E_c + E_{T_i} \tag{9}$$

which corresponds to a mean energy per nucleon

$$W(\rho,T) = m_o c^2 + E_c + \sum_i \lambda_i (E_{T_i} + E_i) \tag{10}$$

where the mean thermal energy per baryon is

$$E_T = \sum_i \lambda_i\ E_{T_i} \tag{11}$$

and

$$\Delta M\, c^2 = \sum_i \lambda_i\ E_i \tag{12}$$

is the mean additional rest mass due to the occupation of the resonances with $m_i > m_o$. The inclusion of a free pion gas (Stöcker,1978) with energy

$$E_\pi = \frac{g_\pi}{e^{\frac{m_\pi c^2 - \mu_\pi}{T}} - 1} \cdot m_\pi c^2 + \frac{4\pi\, g\pi}{(hc)^3 (2\pi)^3}\, V \int_{m_\pi c^2}^{\infty} \frac{d\varepsilon\ \varepsilon^2 \sqrt{\varepsilon^2 - m^2}}{e^{\frac{\varepsilon - \mu}{T}} - 1} \tag{13}$$

is of little importance at lower temperatures because most of the pions stem from the decay of the Δ resonance only. The direct production of pions due to thermal nucleon-nucleon collisions has also been studied, but will be reported elsewhere (Stöcker,1979a).

The pressure is evaluated from the relation

$$p = -\left(\frac{\partial E}{\partial V}\right)_s = \rho^2 \left.\frac{\partial\, W(\rho,T)}{\partial \rho}\right|_s . \tag{14}$$

Taking the pure nucleon gas only, we immediately obtain

$$p = p_c + p_T = \rho^2 \frac{dE_c}{d\rho} + \rho^2 \frac{\partial E_T(\rho,\sigma)}{\partial \rho}\Big|_\sigma \quad . \tag{15}$$

For the compression energy we obtain the compression pressure

$$p_c = \frac{K_o}{18\rho_o} (\rho^2 - \rho_o^2) \quad . \tag{16}$$

The thermal pressure of the Fermi gas is given by

$$p_T = \frac{1}{3} \beta^{-1} \sigma^2 \rho^{5/3} = \frac{1}{3} \beta \rho^{1/3} T^2 \tag{17}$$

which leads to the relation

$$p_T = \frac{2}{3} \rho E_T \quad . \tag{18}$$

This relation, however, is not only valid for the low temperature limit, but also for the zero temperature Fermi gas and, non-relativistically, for any finite temperature. This relation is, in fact, also valid for a classical ideal gas as can be seen directly from $p V = N k T_k$ which is equivalent to $p = \rho \cdot T$ and with $E_T = 3/2 \quad T$ one has $p = 2/3 \rho E_T$.

For an ultra-relativistic gas ($\varepsilon/m >> 1$) the analogous relation $p_T = 1/3 \rho E_T$ holds again as well for a classical as a Fermi gas (even for $T_F = 0$). Therefore one has in this case $E_T = 3T$.

Knowing the pressure and the energy density $e = \rho W$ we can calculate the sound velocity in nuclear matter

$$c_s/c = \left(\frac{\partial p}{\partial e}\right)^{1/2}\Big|_\sigma \tag{19}$$

which for groundstate nuclear matter ($\rho = \rho_o$, $T = 0$) is connected directly to the compression constant (see Fig. 3)

$$K_o = 9 \rho_o^2 \frac{\partial^2 E_c}{\partial \rho^2}\Big|_{\rho_o} \tag{20}$$

via $$c_s/c = \left\{ \frac{K_o}{9W_o} \right\}^{1/2} \sim 0.1 - 0.2$$

5. PHASE TRANSITION OF NUCLEAR MATTER IN HIGH ENERGY HEAVY ION COLLISIONS

One of the most intriguing motivations for investigating relativistic heavy ion collisions is the possibility that phase transitions occur in highly dense nuclear matter, which eventually can lead to stable, abnormally dense nuclei called density isomers. A lot of theoretical investigations on this subject have been undertaken: Feenberg (1945) and Primakoff discussed the possibility of a transition of normal nuclear matter into a superdense "collapsed" tightly bound nucleus, with a total mass close to zero and therefore with enormous binding energies. They argued that this phase transition may occur due to strong nuclear tensor forces or short-range attractive many-body forces. The collapsed state should be separated from the normal ground state by a large potential barrier, which practically prevents the transition into the new state of matter. They also mentioned at first the possibility of collapsed transuranic (i.e. superheavy) nuclei, and briefly

discussed highly deformed states and very large spin states. 20 years later Ne'eman (1974) considered a similar effect: The existence of an attractive inner part in the hard-core nucleon-nucleon interaction may lead to the appearance of strongly bound dense nuclei.

Independently of both former ideas, Bodmer (1971) proposed to look for collapsed light nuclei with large baryon numbers, behaving like new elementary particles.He suggested that these objects may consist of a dense system of tightly bound quarks, so that a soft repulsive core might be responsible for their existence. A series of publications were initiated by Migdal (1972) when he proposed the formation of abnormal nuclear states due to pion condensation. Theoretically, the onset of pion condensation is often described as the decay of the Hartree-Fock ground state into ordered zero frequency (i.e. zero energy) particle-hole states carrying pionic quantum numbers. In the new phase at high density the ground state nuclear matter consists of nucleons forming a spin-isospin lattice(Irvine, 1975). This phenomenon may also be interpreted as a phase transition from the nuclear liquid to a nuclear spin-isospin crystal. Or in other words, the phase transition to the abnormal state takes place as a strong collective pion mode appearing above a critical density $\rho_c \gtrsim \rho_o$ with the pion field acquiring a finite ground state expectation value. The pion condensate leads to a lowering of the total energy per nucleon with respect to normal nuclear matter. This is due to the strong, attractive p-wave pion-nucleon interaction. Later on it was found that the inclusion of nuclear correlations and the effects of pion s-waves and $\Delta(3/2,3/2)$ interactions shifts the critical density ρ_c, at which the normal ground state of nuclear matter decays into the spin-isospin ordered system, to higher densities $\rho_c \gtrsim 1.5\ \rho_o$.(Migdal,1972; Brown,1975,1976; Migdal,1978).

It is very essential to note that the perturbation expansion and therefore the RPA approximation completely break down if the system undergoes a phase transition. We therefore propose a method which allows the possibility of a phase transition and which is capable of allowing calculations beyond the phase transition point. (Mattuck,1968).

In the following we will use the effective particle-hole interaction of Migdal (Migdal,1967):

$$\left(\frac{d\rho}{d\varepsilon_F}\right)_{\rho=\rho_o} \qquad U = f_o + f_o' \vec{\tau}_1\cdot\vec{\tau}_2 + g_o \vec{\sigma}_1\cdot\vec{\sigma}_2 + g_o' \vec{\tau}_1\cdot\vec{\tau}_2\,\vec{\sigma}_1\cdot\vec{\sigma}_2 \tag{1}$$

In the momentum independent limit we use,this interaction corresponds to a zero range force in ordinary space. The constants f_o, f_o', g_o, g_o' can be calculated from elementary processes (π,ρ,ω ..... exchange). (Anastasio,1977).

Furthermore we define the nucleon propagator as

$$G(\vec{1},\omega) = \frac{1}{4}\,[\, g(\vec{1},\omega) + \vec{\sigma}\cdot S(\vec{1},\omega) + \vec{\tau}\cdot\vec{T}(\vec{1},\omega) + (\vec{\tau}\cdot\vec{T}(\vec{1},\omega)(\vec{\sigma}\cdot\vec{S}(\vec{1},\omega))\,] \tag{2}$$

where $g(\vec{1},\omega)$, $\vec{S}(\vec{1},\omega)$, $\vec{T}(\vec{1},\omega)$ are functions which have to be determined self-consistently from the Dyson equation

$$G(\vec{1},\omega) = [\, G_o^{-1} - \Sigma_{HF}\,]^{-1} \tag{3}$$

where $G_o^{-1} = \omega - (\varepsilon_k - \mu) + i\delta$ is the free propagator with $\varepsilon_k = \frac{k^2}{2m}$ and the chemical potential μ . Σ_{HF} is the self-energy in Hartree-Fock approximation, i.e.

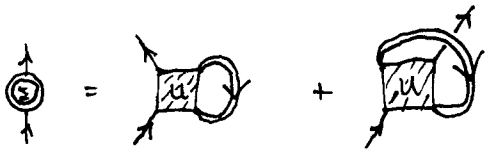

(4)

The direct part is given by

$$\Sigma_{dir} = -i \int \frac{d^3 \vec{l}}{(2\pi)^3} \frac{d\omega}{2\pi} \, tr \, [U \, G \, (\vec{l},\omega)] \, e^{-i\omega o^-} \tag{5}$$

It has to be stressed at this point that denotes the full propagator which is a matrix in spin-isospin space; it has diagonal elements which do not change spin or isospin but in addition has off-diagonal elements which describe spin or isospin flip. The off-diagonal elements vanish in the normal phase and are non-zero after the phase transition. This is the reason why the HF approximation does not break down in the condensed phase in our method.

As the observables e.g. ρ (particle density) and $\vec{\Sigma}$ (spin density) are given by

$$\begin{aligned} \rho &= -i \int \frac{d^3\vec{k}}{(2\pi)^3} \frac{d\omega}{2\pi} \, tr \, [\, G(\vec{k},\omega)] \, e^{-i\omega o^-} \\ \vec{\Sigma} &= -i \int \frac{d^3\vec{k}}{(2\pi)^3} \frac{d\omega}{2\pi} \, tr \, [\, \vec{\sigma} G(\vec{k},\omega)] \, e^{-i\omega o^-} \end{aligned} \tag{6}$$

and

$$\begin{aligned} \vec{t} &= -i \int \frac{d^2\vec{k}}{(2\pi)^3} \frac{d\omega}{2\omega} \, tr \, [\vec{\tau} G(\vec{k},\omega)] \, e^{-i\omega o^-} \\ p_{ik} &= -i \int \frac{d^3\vec{k}}{(2\pi)^3} \frac{d\omega}{2\pi} \, tr \, [\tau_i \sigma_k \, G(\vec{k},\omega)] \, e^{-i\omega o^-} \end{aligned} \tag{7}$$

the total self-energy (direct and exchange) is

$$\Sigma_{HF} = F_1 \rho + F_2 \sigma^i \Sigma_i + F_3 \tau^i t_i + F_4 \tau^i \sigma^k p_{ik} \tag{8}$$

where

$$\begin{aligned} F_1 &= \tfrac{1}{4} [3 f_o - f_o' - g_o - g_o'] \\ F_2 &= \tfrac{1}{4} [5 g_o - f_o - f_o' - g_o'] \\ F_3 &= \tfrac{1}{4} [5 f_o' - f_o - g_o + g_o'] \\ F_4 &= \tfrac{1}{4} [3 g_o' - f_o + f_o' + g_o] \end{aligned} \tag{9}$$

As we are mainly interested in the spin-isospin degree of freedom, we disregard for the moment the spin-spin and isospin-isospin part in Σ_{HF}. If we no insert Σ_{HF} into the Dyson equation we can easily solve for the unknown functions

$$g(\vec{1},\omega) = \frac{4F}{(F - F_4\, p)(F + F_4\, p)} \tag{10}$$

and

$$P(1,\omega) = \frac{4F_4}{(F - F_4\, p)(F + F_4\, p)} \tag{11}$$

where p is the only non-vanishing component (after rotation in spin-isospin space) of the tensor p_{ik} and $F = \omega - (\varepsilon_K - \mu) + i\delta - F_1 N$. With $\tilde{\alpha} = 3f_o - f_o' - g_o - g_o'$ and $\tilde{\beta} = f_o - f_o' - g_o - 3g_o'$, $g(\vec{1},\omega)$ and $P(1,\omega)$ can be integrated with respect to $\vec{1}$, yielding after elimination of μ by means of particle number vonservation the self-consistent equation for the spin-isospin magnetization $M = p/N$

$$\frac{\beta\,\rho}{2\varepsilon_F} = \frac{1}{M}\left[(1+M)^{2/3} - (1-M)^{2/3}\right] \tag{12}$$

with $\beta = \tilde{\beta}\left(\frac{d\varepsilon_F}{d\rho}\right)_{\rho=\rho_o}$ so that the actual density dependence of the left side is

$$\frac{\beta\,\rho}{2\varepsilon_F} = \frac{1}{3}\,\tilde{\beta}\left(\frac{\rho}{\rho_o}\right)^{1/3} \tag{13}$$

where $\tilde{\beta}$ is density independent.

Different magnetization curves are shown in Fig. 5. To decide whether the condensed state M = 0 yields lower energy than the normal state M = 0 we calculate the

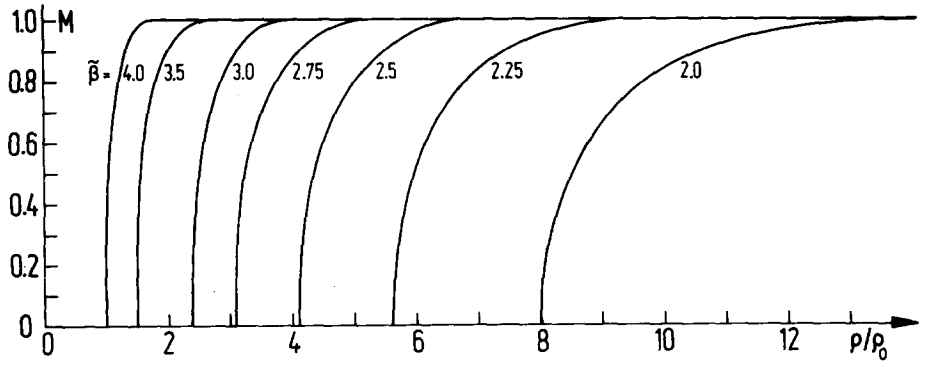

Fig. 5. The density dependence of the spin-isospin magnetization for different values of $\tilde{\beta}$ is depicted.

energy per particle as

$$\frac{E}{N\epsilon_F} = \frac{3}{10}\left[(1+M)^{5/3} + (1-M)^{5/3}\right] + \frac{1}{4}\left[\frac{\alpha\,\rho}{2\epsilon_F} - \frac{\beta\,\rho}{2\epsilon_F}\,M^2\right] \qquad (14)$$

To get lower energy we see that $\beta > 0$ is required. In Fig. 6 we show the actual condensation energy for different values of β. As we neglect spin-spin and isospin-isospin interactions β is essentially given by $\beta = f_0 - 3g_0'$. As for normal nuclei ($\rho = \rho_0$) $f_0 = 1$ and $g_0' \sim 0.7$ there is certainly no phase transition. Nevertheless the momentum dependence of the pion-nucleon interaction induces a renormalization (Migdal,1978) of g_0' yielding values from $\beta \sim 2$ to $\beta \sim 4$. This momentum dependence induces a periodic magnetization instead of a spatially constant one, i.e. we recover the structure of the pion condensate as a spin-isospin lattice. To decide whether there is really a second minimum in the energy per particle as function of ρ we need the E/A (ρ) curve for the normal nuclear state in order to add the condensation energy. Several results are shown in Fig. 7. For

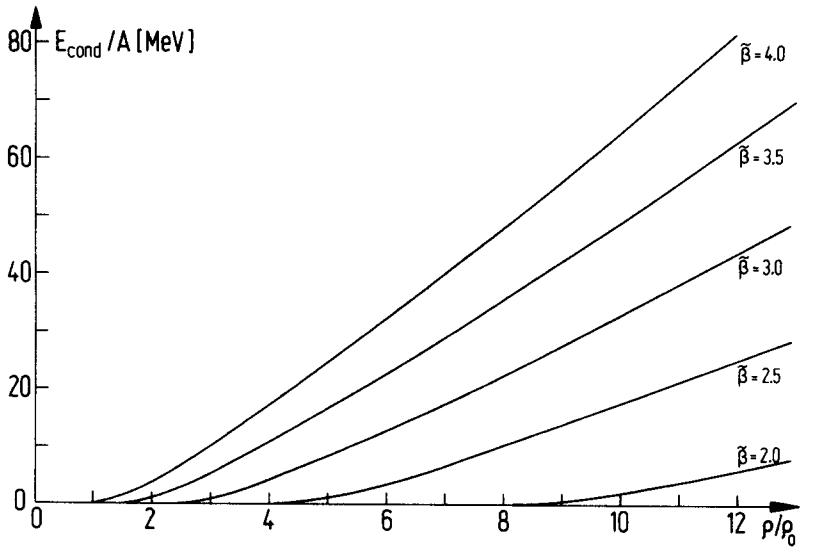

Fig. 6. The condensation energy as function of the density for different values of $\tilde{\beta}$.

reasonable values of $\tilde{\beta} \sim (2\text{-}4)$ an extreme softening of the equation of state can be observed. At least a van der Waals type of behaviour can be seen, yielding a minimum of the pressure as function of ρ. If the phase transition occurs at rather low density ($\rho/\rho_0 \sim 1.5$) a rather broad second minimum may occur allowing extremely high compression of nuclear matter. At reasonable value of $\tilde{\beta} \sim 3$ we observe a density isomer at about $\rho/\rho_0 \sim 5\text{-}6$ with absolute binding energy of $E/A \sim -13$ MeV (Fig. 8). The phase transition actually starts at $\rho/\rho_0 \sim 2.8$ even lower than the barrier maximum at about -10 MeV. Finally we may summarize that a proper treatment of the spin-isospin phase transition in the framework of the Landau-Migdal Fermi-liquid theory yields a density isomeric state at moderate densities of about $2 \leq \rho/\rho_0 \leq 6$ with an energy gain of 20-40 MeV per nucleon. At this low densities the phase transition region (from ρ_{cr}/ρ_0 to $\rho(M=1)/\rho_0$ (see Fig. 9)) is rather narrow, so that the condensation can be achieved in a time which is

short compared to the collision time.

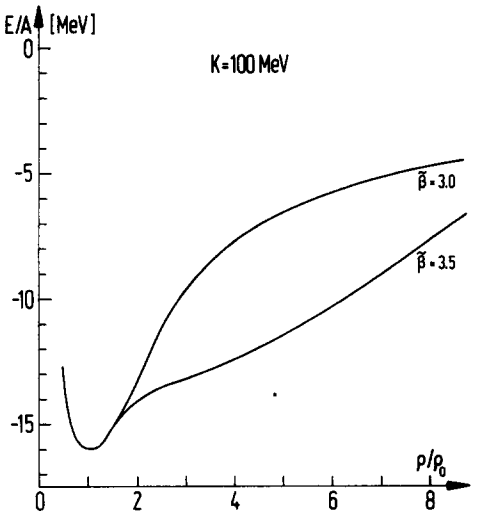

Fig. 7. The nuclear equation of state with spin-isospin condensation shows an extreme flattening at higher densities.

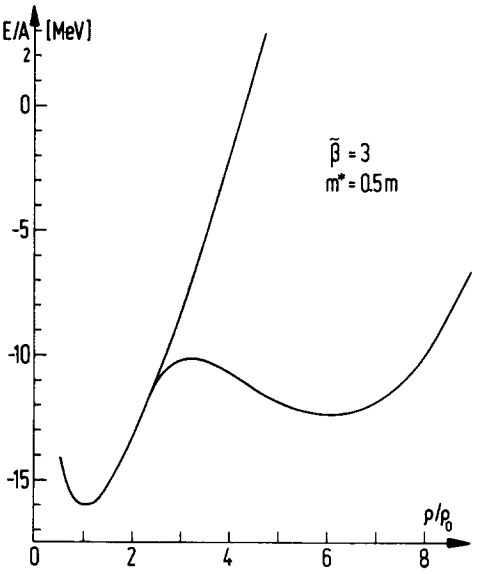

Fig. 8. The equation of state develops a second minimum for an effective nucleon mass $m^* = 0.5$ m.

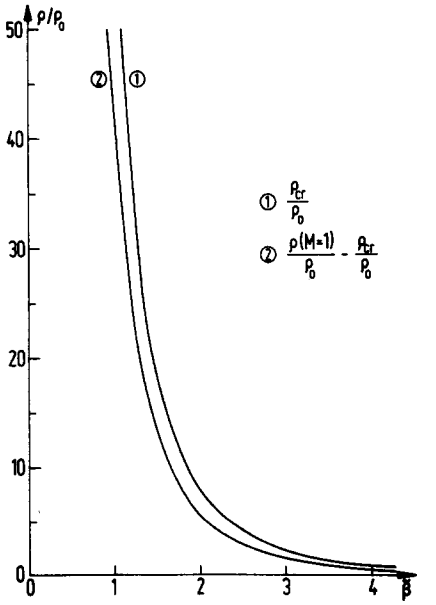

Fig. 9. The critical density and the width of the phase transition are shown as function of $\tilde{\beta}$.

The only possibility to reach such high densities in the lab seems to be violent collisions of heavy ions. This raises the question, whether the high nuclear excitations one expects for these collisions will destroy the ordering effect of this pion condensate. This has been investigated by Ruck, Gyulassy and Greiner. They found that finite size and short time scale are sufficient to allow for pion condensation (Ruck,1976) Gyulassy and Greiner (1977) modified the p-wave part of the pion polarization operator to include the nuclear temperature by a smeared out Fermi distribution of the nucleons (see also the later treatment of Weise and Hecking,1979). They find that the density dependent critical temperature T_c, above which the thermal distributions destroy the ordered spin-isospin lattice lies substantially above that expected from hydrodynamic calculations (see Fig.10)

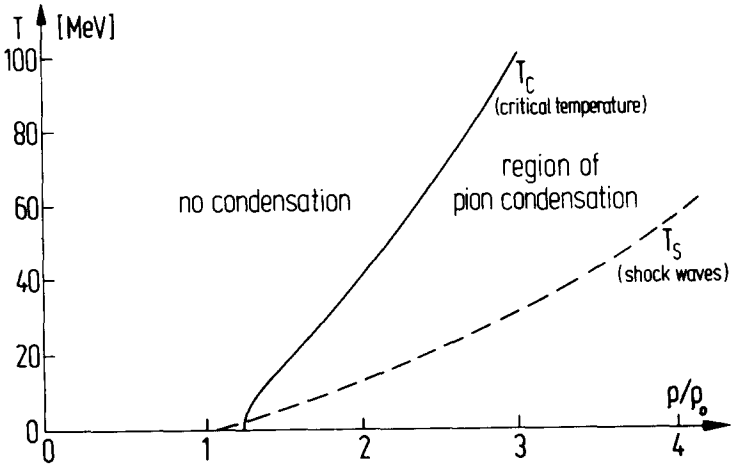

Fig. 10. The critical temperature T_c, above which pion-condensation does not occur. T_s indicates the temperature occurring in shock waves.

As the condensate occurs at finite momentum $k_c \sim 2m_\pi$, the critical distance $R_c \sim k_c^{-1}$ $\sim$ 1 fm. Thus a dense system of dimension $\tilde{\sim}$ 2 fm could support a condensate. The relaxation time of the pion condensate can be estimated from $\tau_{cond}^{-1} = \max|2 \text{ Im } \omega|$, where ω is the complex zero of the pion propagator Δ_π in nuclear matter. This gives $\tau_{cond} \sim 1/5\ \tau_{coll}$ indicating that a condensate can develop during the collision time. The occurrence of a pion condensate is also connected with the critical scattering of nucleons at densities in the vicinity of the phase transition. In fact, the observed strong increase of the n-n scattering (see later) may also be used as an experimental signal for the onset of pion condensation.

Lee (1974) and Wick suggested within the σ-model Lagrangian field theory that the restoration of chiral symmetry can result in very small nucleon rest masses. The practically massless nucleons forming strongly bound nuclei with binding energies of 140-500 MeV/n,i.e. an order of magnitude larger binding effects than in normal nuclear matter. The ground state of this abnormal phase is expected at $\rho \gtrsim$ 2-5 ρ_o. The total energy of the abnormal nucleus consists of the nucleon kinetic energy and a potential energy term arising from the σ-meson field energy. In central collisions of e.g. two Uranium nuclei even the formation of superheavy superdense nuclei seems feasible.

Such an abnormal nucleus can have completely different properties from a normal nucleus: Due to the probably totally different mass defect the atomic mass will not be an integer number. Furthermore, a collapsed (superdense) superheavy nucleus will have interesting atomic properties. Fig. 11 shows the electronic binding energies of collapses superheavy nuclei as function of the nuclear density as calculated by J. Reinhardt. (Stöcker,1978a). One sees that for large Z the binding energy exceeds twice the electron rest mass - an empty electron state will then be filled by an electron from the Dirac Sea, accompanied by the production of positrons without expenditure of energy. This process manifests the spontaneous decay of the neutral vacuum into a charged vacuum. If in a fast nuclear collision collapsed superheavy nuclei are formed, the exotic atomic properties may help in the identification of long lived or even stable collapsed superheavy nuclei via the emission of high energy characteristic X-rays or - better - by searching for sharp resonances in the positron scattering cross section. These observations would yield precise information on the nuclear charge density of an abnormal nucleus.

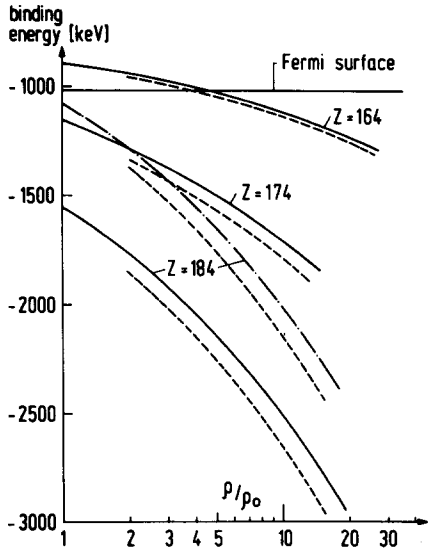

Fig. 11. The electronic binding energy as function of the nuclear density is shown.

6. QUARK MATTER AS A SPECIAL PHASE OF HADRONIC MATTER

The strong compression available in nuclear collisions at very high bombarding energies may serve as a tool to form a new form of matter: If the nuclear matter is so dense that the nucleons overlap strongly it is possible and may be energetically more favourable that not only the nuclei, but also the nucleons desintegrate.

When the nucleons dissolve into their constituents, the partons, which are believed to be quarks, the formation of a multi-quark object is feasible (Collins,1975; Baym,1976; Keister,1976). We will investigate the possible quark phase within the pheonomenological MIT-quark bag model: (Chodos,1974).

One can show that the simple model of a bag - which must be viewed as a volume in space, in which massless quarks move quasi-free - can fit the mass spectrum of

the light hadrons quantitatively quite convincingly, if the following conditions are fulfilled: a) The bag, i.e. the volume in which the quarks move, has a constant positive energy density, which therefore increases infinitely with the bag volume. This bag energy accounts for the quark confining potential, which does not allow the separation of single quarks from each other. b) The zero point motion has to be included for quarks which move within the small volume of a hadron. c) The energy of the quarks is included by solving the Dirac equation for a bound quark state inside the bag. d) Low-order terms in the quark-gluons coupling constant are additionally included to take into account the mutual interactions more realistically.

For our test calculations on the formation of a "Giant Quark Bag" we assumed that the bag energy density constant remains unchanged if the hadronic matter "fuses" into the Giant Quark Bag volume. We neglect the zero point motion, as the GQB is supposed to be much larger than a hadron bag. For the kinetic energy of the quarks we used the free, massless "ultra-relativistic" ($p = 1/\rho \;\; \rho \;\; E_T$) Fermigas model which for zero temperature yields

$$E_{F_Q} = \frac{3}{4} \left(\frac{6\pi^2}{g_Q} \right)^{1/3} \hbar c \;\; \rho_Q^{\,1/3} \quad . \tag{1}$$

From the quark Fermi energy, the Fermi pressure may easily ba calculated as $p_F = \rho^2 \left. \frac{\partial E}{\partial \rho} \right|_\sigma$ which yields

$$p_{F_Q} = \frac{1}{4} \left(\frac{6\pi^2}{g_Q} \right)^{1/3} \hbar c \;\; \rho_Q^{\,4/3} \quad . \tag{2}$$

Thus, the fermi energy and -pressure of the quark gas are related

$$p_{F_Q} = \frac{1}{3} \;\; p_Q \;\; E_Q \quad . \tag{3}$$

The latter relation does not only hold for T=0, but is actually valid for all temperatures. The interaction of the quarks can be calculated and leads to an effective $\lesssim$ 50% rise of the density-dependent Fermi energy (Stöcker,1977).

The density-dependent ground state energy of the Giant Quark Bag is then given by

$$E_{BAG} = \sum_Q \left(\frac{B}{\rho_Q} + \frac{3}{4} \left(\frac{6\pi^2}{g_Q} \right)^{1/3} \hbar c \; (1+\alpha_c) \rho_Q^{\,1/3} \right). \tag{4}$$

E_{BAG} is depicted in Fig. 12. It is shown, that near the normal ground state of nuclear matter, with the parameters used by Chodos(1974) et al. the GQB energy is approximately $\lesssim$ 300 MeV/n above the nuclear matter curve;here we used B = 56 MeV and α_c = 0.5. The statical factor g_Q for a quark gas with spin, flavour and colour (g_Q = 12) was used. However, for smaller B and α_c, this difference is much smaller and the Quark energy may be lower than that of nuclear matter, already at rather moderate densities, if a rather stiff, i.e. quadratic compression interaction is used for the nucleons.

In our investigation we have up to now not taken into account the density dependence of α_c (Freedman,1978).

$$\alpha_c(k) = \frac{12\pi}{33-2n_f} \;\; \frac{1}{\ln\,(k^2/\Lambda^2)} \quad .$$

If we replace $k \to k_F$ we induce a density dependence

$$\alpha_c(\rho) = \frac{12\pi}{33-2n_f} \quad \frac{1}{\ln\{(\frac{6\pi^2}{g})^{2/3} \frac{(\hbar c)^2}{\Lambda^2} \rho^{2/3}\}} \quad ,$$

i.e. $\alpha_c \to 0$ if $\rho \to \infty$. Detailed calculations by Freedman (1978) et al. show, that $\alpha_c \sim 0.5$ at low baryon densities and $\alpha_c \sim 0.1$ already at $\rho_{nuc} \sim 6\ \rho_o$. We therefore expect to be on the $\alpha_c = 0$ curve at high densities. This density dependence of α_c lowers the phase transision point considerably.

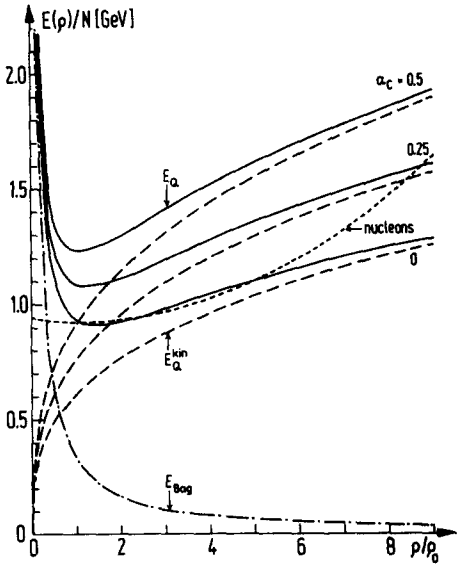

Fig. 12. The energy per nucleon for a quark gas is shown for a bag constant B = 56 MeV and different values of α_c. The nuclear equation of state is shown (dashed curve).

The quark matter equation of state can be put into the relativistic shock equation (3.8) to yield the thermodynamic variables for a dense quark gas when it is formed in a relativistic heavy ion collision.

To solve the relativistic shock equations, the free enthalpy and pressure

$$I = \rho E_F + B + p \tag{5}$$

$$p = p_F - B \tag{6}$$

have to be inserted into equation (3.8), where remaining "undissolved" nucleons are neglected. Then the following equation is obtained:

$$E_F^2 - W_o^2 + p_F \left(\frac{E_F}{\rho} - \frac{W_o}{\rho_o}\right) + B \left(\frac{W_o}{\rho_o} + \frac{E_F}{\rho} + \frac{p_F}{\rho^2}\right) = 0 \quad . \tag{7}$$

Here the last part gives the influence of the Bag itself. Using $p_F = \frac{1}{3} E_F$ for the quark gas, eq. (7) can be solved analytically to yield

$$E_{cm} = \frac{1}{2} \left(\frac{1}{4} W_o \, {}^{B}/_{\rho_o} + {}^{\rho}/_{\rho} + \left(\left(\frac{7}{4} W_o \, \rho/_{\rho_o} - {}^{B}/_{\rho}\right)^2 - 3 W_o \left(\left(\rho/_{\rho_o}\right)^2 - 1\right)\right)^{1/2}\right). \tag{8}$$

From this equation the quark density within the compression zone is obtained as function of the bombarding energy (see Fig. 13). For B=0 this equation reduces to

$$\frac{E_{cm}}{W_o} = \frac{1}{2} \left(\frac{1}{4} \rho/_{\rho o} + \sqrt{3 + \frac{1}{16} \left(\rho/_{\rho o}\right)^2} \right) \tag{9}$$

These results are also applicable for e.g. Lee-Wick matter and prescribe the upper limit of the compression in the ultra-relativistic regime.

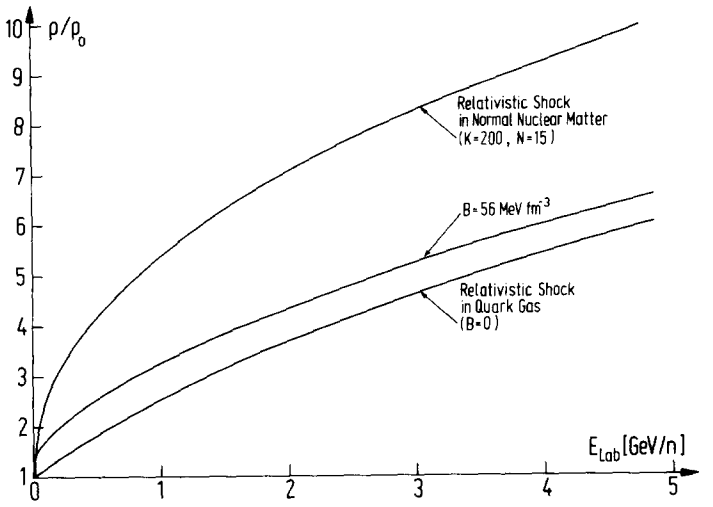

Fig. 13. The actual density achieved in a shock wave in quark matter as function of the bombarding energy.

Due to the large Fermi pressure of the quark gas, its compression increases much slower with the bombarding energy than in the case of nuclear matter. The large ground state energy of the GQB could be responsible for another effect: If at high bombarding energy the nucleons desintegrate and a GQB is formed, the excitation energy of the system mostly has to go into the quark Fermi energy, which can reduce the temperature of the system considerably. Also the distribution of the residual thermal energy over three times as many degrees of freedom will lower the temperature.

In a three-dimensional hydrodynamical test calculation we found that the quark matter is only transiently produced in the collisions of fast nuclei for a very short

time. However, it is possible that part of the quark matter does not immediately recondensate into hadronic matter, but stays within the quark phase for a longer time. This piece of quark matter then expands freely into the state of minimum energy at ρ_o . The expansion will approximately follow curves of constant entropy, Q for which

$$p \cdot V^{4/3} = \text{const and } E \sim \rho^{1/3} \quad \text{(for all T!)} \; . \tag{10}$$

Such a metastable GQB would have a ground state density different from the nuclear equilibrium density. It can decay by the sudden release of a large amount of energy (~ 300 MeV/n) into a bulk of normal hadronic matter, hopefully a considerable time after the collision: This may open a way of detecting GQB's. The resulting "hadronic nucleus" may have a rather unique structure, e.g. consisting of many resonances.

Furtheron it seems worthwhile to investigate the possibility of condenstion phenomena due to the colour degrees of freedom of the quarks, which mediate a colour quark-quark interaction.

This colour interaction may be written as (Dalitz,1976)

$$U = f(k) \sum_{i=1}^{8} \lambda^i \lambda^i$$

where $$f(k) = 4\pi \, \alpha_c(k) \, \frac{1}{k^2}$$

with $$\alpha_c(k) = \frac{12\pi}{33-2n_f} \quad \frac{1}{\ln(k^2/\Lambda^2)}$$

which is the QCD fine-structure constant and n_f = is the number of light flavours The definite structure of $\alpha_c(k)$ as function of the momentum k is only vaguely known from renormalization group arguments: (Freedman,1978)for $k \to \infty$ it is expected that $\alpha_c \to 0$ (asymptotic freedom at high densities). At low densities α_c should become large (non-perturbative region of colour confinement).

The expression for $\alpha_c(\,)$ given above fits the large k region quite well. The cut-off parameter has been determined from charmonium data to be of the order of $\Lambda \sim$ 300-500 MeV (Richardson,1979). As we treat the quarks in Fermi gas approximation, we replace k by the Fermi momentum k_F thus inducing a density dependent interaction. This corresponds to the assumption that the medium screens the long range quark-quark interaction as in the case of an electron gas.

With the quark propagator

$$G(k,\omega) = \frac{1}{3} \left[g(k,\omega) + \lambda^i \lambda_i (k,\omega) \right]$$

we calculate the Hartree-Fock self-energy

$$\Sigma_{HF} = \frac{2}{g} f \rho - \frac{1}{3} f \; d_{iik} C^k$$

$$- \frac{1}{2} \left[- \frac{4}{3} f \; Cm + \frac{2}{3} f \; d_{iim} \rho \right.$$

$$\left. + f \, (if_{ikj} + d_{ikj})(if_{jim} + d_{jim}) \, C^k \right] \lambda^m \; .$$

where f_{ijk} and d_{ikj} are the $SU_c(3)$ structure constants and $C^k(k=1,\ldots,8)$ is the integrated colour density

$$C_k = \frac{2}{3}\, i \int \frac{d^3k}{(2\pi)^3} \quad \frac{d}{2\pi} \Lambda_k\ (h,\omega)\ e^{-i\omega o^-} \quad .$$

As the colour group $SU_c(3)$ allows to select two diagonal generators e.g. λ_3 and λ_8 (which we call in the following colour-isospin and colour-hypercharge) we investigate e.g. colour condensation in the λ_8-direction. Furthermore we assume the quarks to be massless and treat them as relativistic Fermi gas i.e.

$\varepsilon_F = k_F = (\frac{6\pi^2}{g})^{1/3}\ \rho^{1/3}$ where g is the factor of statistical degeneracy g=12.
Applying now the method developed in the nuclear context we find the self-consistent equation for the colour magnetization by solving the Dyson equation. For the colour-hypercharge magnetization we find with $F_1 = 1/6 - 3)\ f$ and $M_8 = (1/2)\ 3\ C_8/\ \rho$

$$\frac{F_1\rho}{\varepsilon_F} = \frac{1}{M_8} \quad (1 + \frac{M_8}{2})^{1/3} - (1 - M_8)^{1/3}$$

and the energy

$$\frac{E}{\varepsilon_F N} = \frac{1}{4}\ [\ 2(1 + \frac{M_8}{2})^{4/3} - (1-M_8)^{4/3}\ ] - \frac{1}{9}\ \frac{f\rho}{\varepsilon_F} - \frac{1}{6}\ \frac{F_1\rho}{\varepsilon_F} M^2 \ .$$

Expanding $(1 \pm M)^{1/3}$ we find the phase transition point as

$$\frac{F_1\rho}{\varepsilon_F} = \frac{1}{2} \quad .$$

As can be seen from the energy, there is an energy gain through condensation only if $F_1>0$, i.e.

$$F_1 = (\frac{1}{6} - 3\ )\ 4\pi\ \alpha_c\ (k_F)\ \frac{1}{k_F^2} > 0 \quad .$$

We therefore find that there is no net colour magnitization as long as

$$\alpha_c(k_F) > 0 \quad .$$

Our present knowledge (Freedman,1978) from QCD says that $\alpha_c(k)>0$ at all k. Therefore there should be no phase transition at all. Nevertheless it is well known, that the phase transition from a nucleon gas to a quark gas is very broad with the coexistence of a nucleon and a quark phase. Therefore there may be many-body effects changing $\alpha_c(k)$ to an effective $\alpha_c^{eff}(k)$ during this percolation phase. This $\alpha_c^{eff}(k)$ may have negative domains, thus accomplishing colour condensation. As

$$\frac{F_1\rho}{\varepsilon_F} \cong 4\ \alpha_c^{eff}\ (k)$$

already $\alpha_c^{eff} = -\frac{1}{8}$ is sufficient for the colour phase transition to take place.
This type of intermediate colour condensate will enhance the nucleon-quark phase transition due to the condensation energy gain, which is (in the condensed region)

$$\frac{E_{cond.}}{Nucleon} = \tilde{\alpha} \left(\frac{\rho}{\rho_o} \right)^{1/3}$$

with $\tilde{\alpha}$= 73 MeV for $\alpha_c^{eff} = -0.3$. Therefore the nucleon-quark phase transition region at about $5\rho_o$ the actual condensation energy gain is of the order of 125 MeV. We therefore conclude that a phase transition from nucleon to quark matter at densities lower than predicted by bag calculations may be a hint for condensation pheneomena pointing out a deviation from standard QCD. At the phase transition point we expect the well known critical scattering phenomenon (Gyulassy,1977): The scattering cross section is drastically enhanced. This point needs further investigation in the context of quark matter.

7. THE COMPRESSION AND EXCITATION EXPECTED FROM NUCLEAR SHOCK WAVE CALCULATIONS FOR HIGH ENERGY HEAVY ION COLLISIONS

Let us first look for the results of the one dimensional shock calculations of head-on collisions of equal nuclei, which allow the study of the influence of various parameters of the nuclear equation of state on the reaction, mainly on the compression rates and temperatures reached, but also the shock and flow velocities and on the production of pions and nuclear resonances (Baumgardt,1975; Stöcker, 1978). The compression rate in the rest frame of the compressed matter is shown in Fig. 14. It is found that the compressibility constant is of importance for the compression of the lower energies, where a stiffer equation of state (i.e. larger K-values) results in lower compression. For very high energies, we can neglect the compression energy completely and derive an analytic expression for the asymptotic behaviour of (ρ/ρ_o) asymptotic (E_{LAB}). For an ideal gas $p = 2/3\ \rho\ E_T$ the shock equations reduce to

$$\rho/\rho_o = \frac{1}{2} \left(5 \left(\frac{\gamma_{L+1}}{2} \right)^{1/2} + 3 \right) \qquad (1)$$

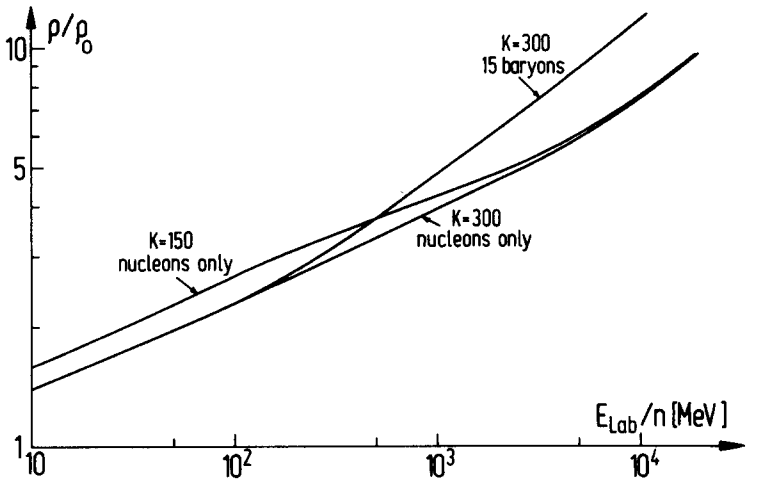

Fig. 14. The compression reached in the rest frame of the compressed matter is shown.

where $\gamma_L = \frac{E_{LAB}}{W_o} + 1$. Therefore, in the relativistic domain, the rest frame compression is not limited to $\rho/\rho_o = 4$ (this was wrongly assumed by various authors (Sobel,1975)) as in the non-relativistic limit ($\gamma_L \approx 1$), but increases with the square root of the bombarding energy. $\rho/\rho_o = 4$ is reached at $E_{LAB} \approx 1$ GeV/n, i.e. just where relativistic phenomena become important.

In the ultra-relativistic limit $\gamma >> 1$, $p = \frac{1}{3}\rho E_T$ one obtains

$$\rho/\rho_o = 4 \cdot \left(\frac{\gamma_L + 1}{2}\right)^{1/2} = 4\ \gamma_{CM} \qquad (2)$$

At the very high energies, the influence of the nucleon resonances dominates. Owing to the increased number of degrees of freedom, the equation of state is softer and therefore higher compression is possible.

Like the compression, the temperature achievable also depends strongly on the nuclear equation of state used. (See Fig. 2). A lower compression constant increases the temperature, as less energy is needed for compression. On the other hand, the inclusion of nucleon isobars decreases the temperature considerably, as the internal excitation goes into the formation of heavy resonances, which means the transformation of thermal energy into additional rest mass. This cooling pheonomenon is what leads to a maximal temperature T^{MAX} in connection with an exponentially increasing hadronic mass spectrum (see later). However, the resonances become important only at densities $\rho/\rho_o \tilde{>} 3$, reached only at relatively high energies. Therefore, the inclusion of resonances is important in the relativistic regime, but may be neglected for moderate energies $E_{LAB} < 400$ MeV/n. At such energies, the feedback of the N^* formation on the system is small and one may consider the $\Delta(3/2,3/2)$ resonance only. In this case the temperature may be calculated for the simple one-phase nucleon gas and from there the resonance excitation can be obtained as in a perturbational treatment. N_Δ/N is then given by the simple formula

$$N_\Delta/N \approx \tau_\Delta\ e^{-E_\Delta/T} = 4\, e^{-\frac{293}{T}} . \qquad (3)$$

We find that thermal pion production is very small for $E_{LAB} \tilde{<} 400$ MeV/n. This means that copious pion production at low bombarding energies will strongly indicate an exotic phenomenon (see later) . The importance of the equation of state for the temperatures attained is seen in Fig. 2, where the temperature obtained in a Fermi gas model is compared to that of a classical ideal gas $E_T = 3/2\ T$ at higher density, the deviations are very large. However, in a relativistic treatment, the Fermion temperature approaches the ideal gas limit for very high temperatures $T \tilde{>} 200$ MeV, as then the Pauli principle can be neglected. Fig. 3 shows the influence of the compression constant on the shock velocity in nuclear matter as a function of the shock amplitude ρ/ρ_o in the matter's rest frame: The shock velocity increases with density and with the compression constant. For small amplitudes, the shock velocities tend to the sound velocity C_s/c, of the ground state, which of course is different for different values of K:

$$C_s/c = \left(\frac{\partial p}{\partial e}\right)^{1/2}_{\sigma=\text{const}} = \left(\frac{K}{9\, W_o}\right)^{1/2} \quad \text{for } \rho = \rho_o \qquad . \qquad (4)$$

For large amplitudes c_s tends to the velocity of light and the influence of K vanishes. If for the thermal pressure an equation of state (or the gas law) different from an ideal gas is used, i.e. for example $\alpha = 1$ instead of $\alpha = 2/3$, $p_T = \rho E_T$ results. The higher internal pressure leads to a much faster increase of $v_s(\rho)$.

Pion Production

To calculate the total pion production rate, one sums over all pions emitted in the decay of the excited resonances and includes the production of the free pion gas. For the strongly compressed state, which is calculated in our model, the formation of temperature-free pions was negligibly small (an order of magnitude down) compared to the Δ-resonance. A comparison with several different model calculations (see Fig. 15) (e.g. pion bremsstrahlung calculation (Vasak,1979), independent nucleon-nucleon collsions (Bertsch,1977), thermal models (Chapline,1973;Heinz, 1978)) does,however, show qualitatively good agreement with the data (Fung,1978). Therefore more refined calculations will be called for interpreting more exclusive experiments. The emission of the pions from the initial, strongly compressed stage during the whole expansion stage, will also increase the number of free pions in the system which is proportional to the volume of the hot matter.

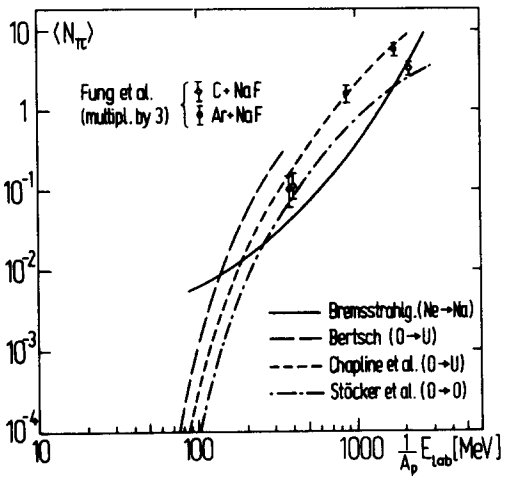

Fig.15. The number of pions produced in a heavy ion collision in different models (see text). Existing experimental results are indicated by points with error bars.

Dependence of the Particle Production on the Nuclear Equation of State.

Within the one-dimensional relativistic shock model, the dependence of the formation of isobars and pions on the nuclear binding energy functional may be investigated by iterative solution of eq.(4.16). In analogy to the influence on the temperature, also the pion production rate strongly reflects the properties density dependence of the compressional energy $E_c(\rho, T=0)$. A soft nuclear equation of state, i.e. small K values, leads to an increasing number of produced particles,as a larger fraction of the internal energy is available for thermal particle production. Thus, the measurement of the rate of increase of the particle production with the bombarding energy may be used to investigate the compression energy $E_c(\rho)$ and the compression constant

$$K_o = 9\,\rho_o^2 \left.\frac{\partial^2 E_c}{\partial \rho^2}\right|_{\rho=\rho_o} \quad \text{and sound velocity} \quad c_s/c = (K/_{9W_o})^{1/2} \tag{5}$$

experimentally. One can also learn about the thermal properties of the nuclear fluid at high temperatures: Using the ansatz $E_T = 3/2\ T$ for an ideal classical gas yields a much faster increase of the shock temperature with the bombarding energy (see also the next sections).

Influence of the Formation of Abnormal Nuclear Matter on Shock Waves.

In the case that a phase transition into a secondary minimum would occur, these results are drastically changed (Hofmann,1979): Above a critical bombarding energy, the matter is compressed to the critical density ρ_c, at which the pressure does no longer increase with the density. If the pressure $p \sim \partial E_c / \partial \rho$ decreases with increasing density, the matter becomes unstable and collapses with no additional need for external compression into the abnormal superdense state. In the region of decreasing pressure no shock waves can be formed, ($v_s \sim p$), i.e. the shock phenomena vanish for this region. This can be used as a signal to detect phase transitions experimentally, namely through the disappearance of Mach shock phenomena. It should be noted that this can be used also to detect inflection points in $E_c(\rho)$, where $p_c(\rho)$ decreases, while no secondary minimum is formed! It was shown by Hofmann(1979) that also an equilibrium coexistence of the normal and abnormal phases, which we excluded because of the short collision times we are considering, does not allow for a stable shock front in the phase transition region - nor for a double-shock as postulated by Galitski (1978).

Another effect of the phase transition is also very important: The collapse of the matter into the abnormal state leads to a sudden release of the condensation energy as additional excitation energy. Thus, a phase transition into a density isomeric state will be accompanied by a strong additional heating of the system, which can be used to observe density isomers in heavy ion collisions independent of the disappearance of Mach shock phenomena, namely by strong threshold increase in the excitation function of the particle production rate (pions, resonances, strange particles - see Fig. 16) and of the high energy tails of the particle spectra, which also reflect the temperature of the emitting source.

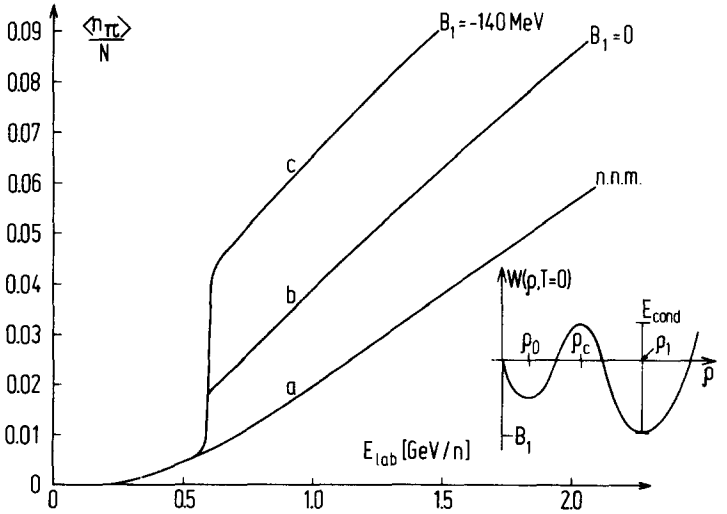

Fig. 16. The influence of a density isomer on the thermal pion production rate is shown.

Expansion and Explosion of the Highly Compressed Matter

The above increase should be observable also when the subsequent expansion of the matter is taken into account. Particles will be emitted during all stages of the reaction from the dense, hot piece of nuclear matter, and mainly from its surface. Two competing processes will lead to the decay of the compressed shock zone: First, the compressed matter will expand isentropically, i.e. with constant entropy. This will result in a collective flow of matter outwards, with the thermal energy per nucleon

$$E_T = \frac{\sigma^2}{2\beta} \rho^{2/3} \tag{6}$$

and the temperature

$$T = \frac{\sigma}{\beta} \rho^{2/3} \tag{7}$$

diminishing with decreasing density, and the kinetic energy per nucleon increasing because of the expansion $E^{kin} = E_{CM} - (E_T + E_c)$ (see Fig. 17). This process continues until the mean distance between the nucleons is too large to ensure thermal contact and equilibrium: The matter breaks then up into pieces. Possibly these break-up densities are reached at densities where the pressure has a minimum ($\rho/\rho_0 \approx 0.5$) which corresponds to a hydrodynamically unstable situation, where the dilute matter condensates into separate fragments.

In the case that abnormal superdense matter is formed, the system retains at larger temperature as compared to the normal matter case (see Fig. 18). As the isentropic curves show the barrier to the secondary minimum even at large temperatures, a trapping of the matter within the abnormal state is possible for a considerably long time. This is discussed in greater detail in the next sections. Secondly, also the possibility of a rapid explosion of the highly excited shock zone has to be taken into account. Since a considerable fraction of highly energetic particles moves faster than the collective outflow described by isotropic expansion, they can quickly escape from the surface of the shock zone.

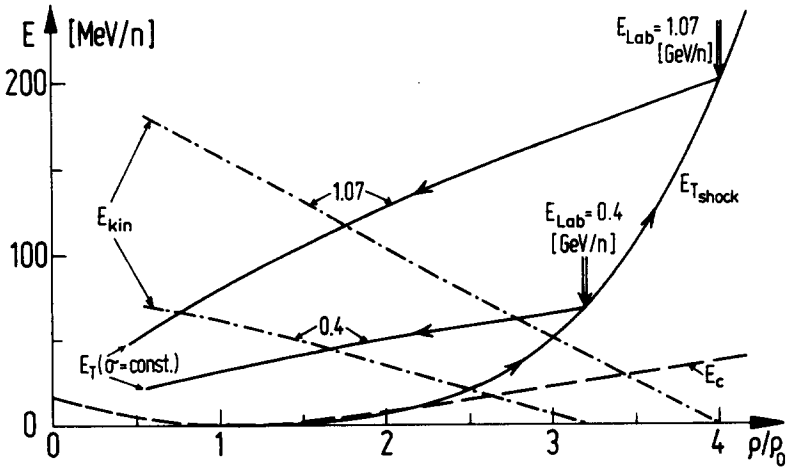

Fig. 17. The reaction kinematics for a heavy ion collision is shown as described in the text.

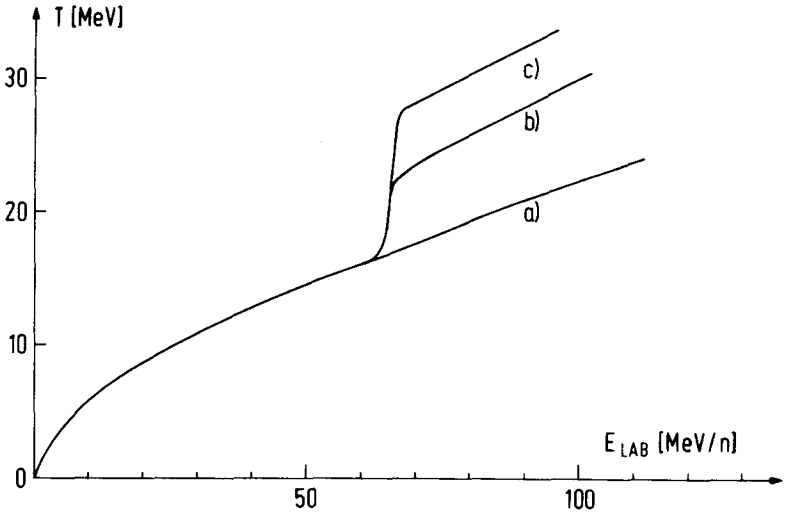

Fig. 18. The energy dependence of the temperature for a) normal nuclear matter, b) density isomer with $B_1 = 0$, c) $B_1 = -140$ MeV.

The vaporization of the surface of the compressed matter (shock zone) will lead to the emission of fast particles, which carry information about the - most interesting- state of highest compression and excitation. Therefore, special emphasis must be given to the observation of the highly energetic radiation components, mainly light, sidewards emitted fragments to learn about the initial compression stage of the reaction. The compressed zone is cooled down via particle radiation, thus slowing down the expansion of the system. The cooling effect, of strong enough, may stabilize an eventually formed abnormal nucleus.

We calculate the expansion of the highly excited matter assuming isentropic expansion of the whole system - the vaporization of the surface of the hot object is presently neglected. Let us, for the sake of simplicity, consider now a pure nucleon Fermigas. Then the thermal energy (6)

$$E_T = \frac{\sigma^2}{2B} \rho^{2/3}$$

for an isentropic expansion (σ= constant) from the state of highest compression in the shock zone to the lower density can be easily calculated: Because of the expansion, the matter cools down as T, $E_T \sim \rho^{2/3}$. The internal energy $E^x = E_c + E_T$ - compression energy and random thermal motion - is transferred into kinetic energy, namely the directed collective outward flow of the system. Fig.17 shows E_T, E_c, and $E_{kin} = E_{CM} - (E_T + E_c)$ as functions of the density for two different bombarding energies $E_{LAB} = 0.4$ and 1.07 GeV/n. The state of highest compression is approached along the shock adiabate, the thermal energy increasing rapidly with the density. In the expansion stage, however, E_T decreases rather slowly with the density, while the kinetic energy of the collective outflow increases very fast, approximately as

$$E_{kin} = E_{CM} (1 - \rho/\rho_o) \qquad (8)$$

where ρ_o is the shock compression. The kinetic energy of the collective outflow is considerably larger than the internal random motion.
Let us now study the time development of the expansion of a homogeneous density distribution in the non-relativistic one-dimensional case, which can be solved

analytically: One can estimate the time dependence of the density which is in our case $\rho = N/R$ from equation (8)

$$\dot{R}(t) = V_{CM} \left(1 - \frac{R_s}{R(t)}\right)^{1/2} \tag{9}$$

where R_s is the radius of the system in the highly compressed state. Separation of variables and integration yields

$$\frac{1}{V_{cn}} \left\{ R \sqrt{R-R_o} + R_o \ln \left(R + \sqrt{R-R_o} \right) - R_o \ln \sqrt{R_o} \right\} = t \, . \tag{10}$$

Fig. 19 shows the compression- and expansion phase for various cases. One notices that a much lower compression than calculated in the shock model does end up in quite a similar final expansion as the shock calculation, only the initial stages are different (dashed line).

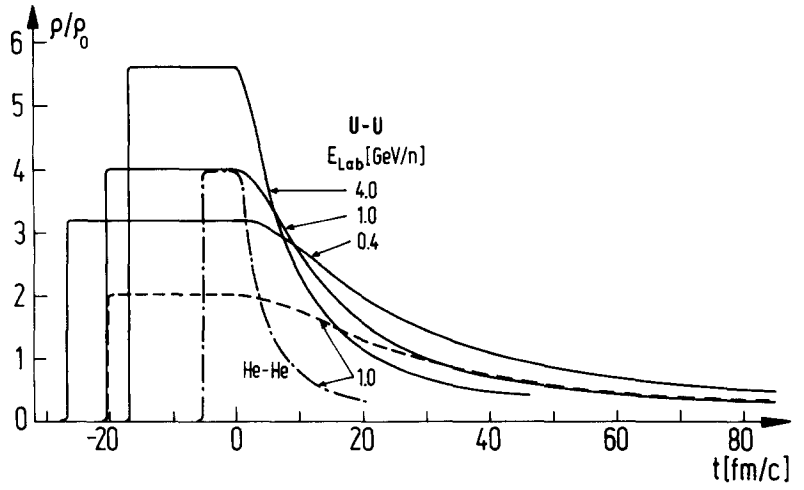

Fig. 19. shows the compression and expansion phase in non-relativistic one-dimensional model.

Another result is the much slower decrease of the density, when a lower bombarding energy is investigated. Finally, the decrease of the density proceeds much faster when collisions of small nuclei are investigated. Therefore, most interesting are central collisions of heavy nuclei, as here the system stays for the longest time in the highly compressed stage $\rho > 2\rho_o$, namely 47 and 36 fm/c for U-U collisions at 0.4 and 1.07 GeV/n. During such a long time, particles (e.g. pions) with $v \approx 0.5$ c can travel 24 and 18 fm respectively, much longer distances than they need to leave the highly compressed zone with $R \approx 8$ fm. This means that one may even obtain information about the compressed center, when the high energy tails of the particle spectra are studied under 90° in the CM-frame: Here the central compression region can be seen without a shadowing effect from the residual projectile- and target nucleus.

Recently, such an experiment was performed by S. Nagamiya (1979) and collaborators in the bombardment of Na F with Ne-projectiles at various energies.

They measured the spectra of the particles (protons and pions) emitted at 90° in the CM frame. They find an exponential decrease of the particle spactra, from which the temperature of the highly compressed zone can be deduced. Fig. 20 shows the results of their measurements (dots). The solid line represents the shock temperature as obtained (without any fit) from the relativistic shock calculations A remarkable agreement between the data and the theory is found; thus the experiment seems to indicate that the shock wave model implying strong compression and high excitation may be valid for the description of study theoretically central collisions of fast heavy nuclei. Furthermore, the experiment shows that it is necessary to use a Fermigas ansatz for E_T (ρ,σ) - a calculation using a classical ideal nucleon gas with $E_T = 3/2\ T$ yields a linear increase of T(E), which strongly contradicts the experiment.

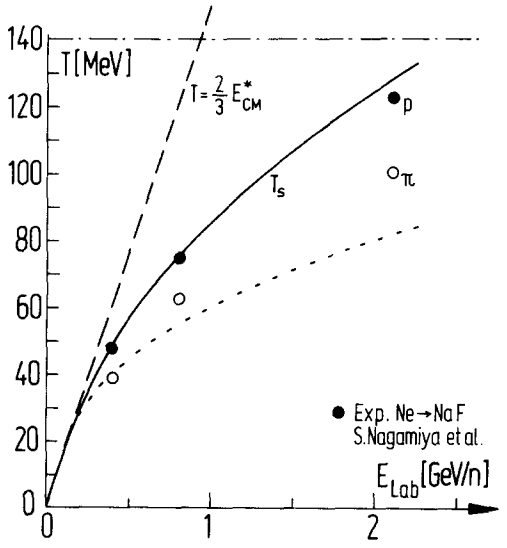

Fig. 20. The proton(full dots) and pion temparatures (open dots) ad deduced from the experiment of Nagamiya et al. compared to the shock calculations for pure nucleon gas (full curve) and including the resonance cooling (dashed curve).

However, the absolute value of the deduced temperature is surprisingly high - one would expect that the matter is cooler due to the resonance - and pion creation. If the curves of Nagamiya (1979) et al. are extrapolated to higher bombarding energies, the limiging temperature (Hagedorn,1965) $T^{Max} \approx m_\pi c = 140$ MeV may be achieved already for $E_{LAB} \sim 3$ GeV/n, i.e. at heavy ion energies,which are presently only available at the synchro-phasotron in Dubna. The possibility of finding temperatures $T > T^{Max}$ is an exciting task for further experiments. According to

recent papers (Fowler and Weiner,1979; Kapusta,1979) the existence of quark matter would not allow for an exponential mass spectrum of elementary particles and thus a limiting temperature would not exist. Another important feature of the data of Nagamiya is the result that the temperature of the pions is systemantically lower than that of the protons. The proton spectra may show up higher energies due to the hydrodynamical outflow of nucleons resulting in an apparently higher temperature. One may also speculate that they arise from a stage cooled because of higher compression energies or finite resonance production, or that the pions are not in a complete thermal equilibrium with the nucleons. Sandoval (1979), Stock, Schroeder and collaborators determined in a streamer chamber experiment the pion production rate in central collisions of Ar on KCl. They measured very large charged particle multiplicities (approximately the sum of the proton numbers of projectile and target) for E_{LAB} = 1-2 GeV/n. They find that the pion multiplicity $\langle m_\pi \rangle$ is of the order of 10-20 per cent of the nucleon multiplicity $\langle m_p \rangle$ increasing approximately linearly with the bombarding energy. Using the temperatures calculated on the basis of the relativistic shock equation, which coincide well with the temperatures measured by Nagamiya, we estimated the number of pions created considering Δ-resonance formation via

$$\frac{\langle m_\pi \rangle}{\langle m_N \rangle} \approx \tau_\Delta \, e^{-E_\Delta/T_s} = 4 \, e^{-E_\Delta/T_s}$$

where $\tau_\Delta = 4$ is the statistical factor of the Δ(3/2, 3/2) resonance. In Fig. 21 the data are compared to the calculations. The experimental data are again similar to the results of the shock calculations.

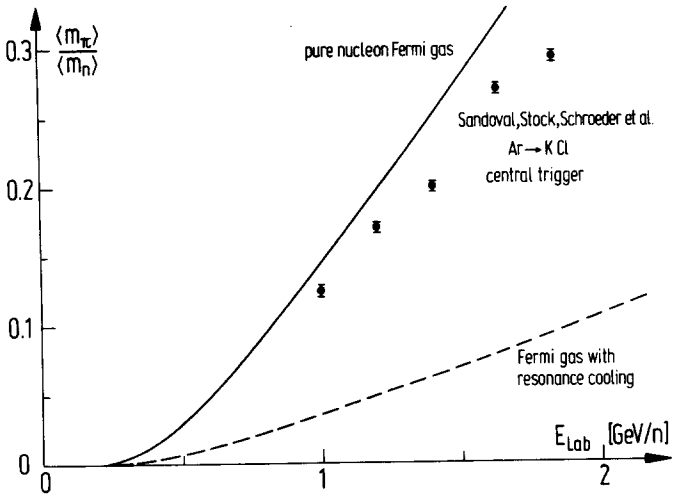

Fig. 21. The pion production rate $\langle m_\pi \rangle / \langle m_N \rangle$ as obtained in the experiment of Sandoval et al. (dots) compared to the shock calculation without resonance cooling (full curve) and including the resonance cooling (dashed curve)

However, again we would expect that the cooling influence of the resonance - and pion formation lowers the temperature, thus leading to a smaller pion production rate than experimentally observed, and to a lower increase of $\langle m_\pi \rangle / \langle m_p \rangle$ with the

bombarding energy (dashed curve). A full relativistic treatment of the resonance production can increase the pion multiplicity obtained in the shock calculation. However, the data point at 1.6 GeV/n is slightly above the straight line. If this result is not due to a statistical error, which cannot be excluded at the moment, an increase of $\langle m_\pi \rangle$ and a change of the slope $\langle m_\pi \rangle$ seems to appear at $E_{LAB} \sim 1.6$ GeV/n. This would be a very exciting result, as it would be interpreted as evidence for phase transition in dense nuclear matter at $\rho/\rho_o \simeq 4\rho_o$. From the apparent jump in the temperature one may deduce the condensation energy of the density isomeric state (i.e. the depth of the secondary minimum in E_c as measured from the barrier at E_c (ρ_c)). However, as long as this effect has not been definitely proven by more extended and refined experiments with better statistics and measuring at the lower energies and in smaller energy bins, this remains speculation - which, nevertheless, may be stimulating also for the forthcoming experiments. In conclusion, already from these simple one-dimensional shock calculations it appears that one can learn about the reaction dynamics and the properties of the nuclear equation of state from high energy heavy ion collisions, if the relevent windows, uniquly reflecting the occurrence of interesting or exotic phenomena, are searched carefully.

The Importance of Nuclear Viscosity and Thermal Conductivity

Let us now turn away from the more schematic one-dimensional shock model to more refined nuclear fluid dynamical calculations: Though the solution of the relativistic shock equations allows for an overview of the phenomena and reasonably enables us to obtain values for the various variables considered, it is highly idealised and does not give an answer to the questions concerning the details of a nuclear reaction at high energies. This is only possible by solving the equations of motion for a non-ideal nuclear fluid numerically. The most important feature of a non-ideal fluid is the occurrence of viscous effects and thermal conductivity - therefore at least equations of the Navier-Stokes type have to be solved. A two and three-dimensional relativistic fluid dynamical model is presently under preparation by G. Buchwald, but not yet available. Therefore we concentrate on the influence of the viscosity in a one-dimensional fluid dynamical model. Within this model we can look somewhat deeper into the details of a heavy ion collision, e.g. study the time dependence of the compression and thermal excitation as well as the possibility of formation abnormal superdense states.

To solve the equations of motion - the non-relativistic Navier-Stokes equations in one dimension - we had to incorporate the nuclear potential and the friction tensor into the Euler equations. The Yukawa potential allows for a realistic treatment of the nuclear surface in that a smooth decrease of the density is obtained. For the friction tensor $\overleftrightarrow{S}$ a one dimensional Newtonian form $\overleftrightarrow{S} = -\eta(\vec{\nabla}\cdot\vec{v})^2$ is used. The friction constant is adjusted to $\eta = 10\ \hbar\ \mathrm{fm}^{-3}$, which ensures numerical energy conservation to $E/E_{KIN} \sim 10\%$. The most important advantage of the viscosity is to smooth the otherwise sharp shock fronts obtained in fast collisions to reasonable width. The formation of resonances and pions was not taken into account in these first calculations.

The integration of the equations of motion was done for various bombarding energies. Density isomeric states with different depths and critical densities were also investigated. For normal nuclear matter we first found a rapid increase of the compression rate in the center of mass, followed by a rather stationary stage of constant compression (corresponding to the shock wave model) - and subsequent expansion stage (see Fig. 22a,b). Within that model we can also look for fusion events (see later). The mean thermal energy increases much more slowly - since for hypersonic projectile and target velocities matter not yet reached by the shock stays practically undisturbed in its ground state (see Fig. 22c)

On the other hand, the compression rates and temperatures obtained in the "stationary stage" are in quite good agreement with the result of the shock calculations

(see Fig. 23a,b) The inclusion of thermal conductivity has the consequance that heat energy is transported away from the most strongly compressed regions - this is of great importance for the formation and stabilization of metastable superdense nuclei.

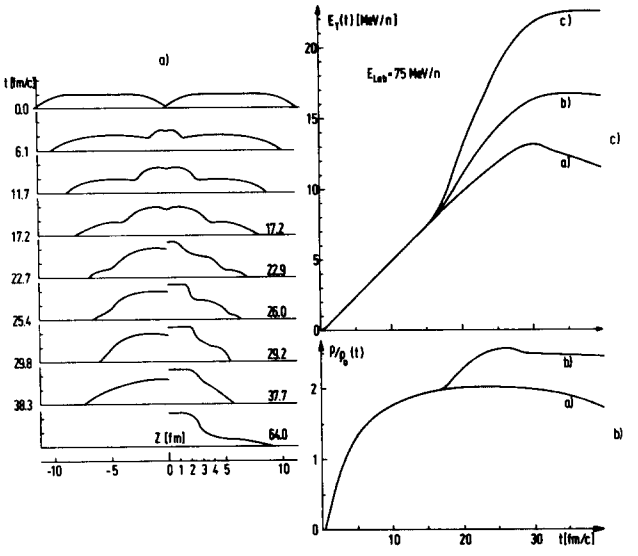

Fig. 22. (a) The density distribution of various stages of a central collision of two equal nuclei E_{lab}=75 MeV/n. The left-hand shows $\rho(z)$ for a normal equation of state K_o=300 MeV/): the second central region quickly expands again. The right-hand side shows the strong density increase in the case of a density isomeric state: a 'large part of the system stays rather long within the abnormal phase (density isomer at $\rho_c = 2\rho_0, \rho_1 = 2.5\ \rho_0, B_1 = 0$).

(b) The central compression $\rho/\rho_0(t)$ increases strongly above the critical density for the production of an isomeric state: compared to the normal nuclear matter (lower curve), the presence of a density isomer leads to the collapse of the nuclear matter into the abnormal superdense phase (upper curve). Thus the matter remains much longer within the strongly compressed state.

(c) The gain of condensation energy leads to a strong increase of the mean thermal energy $E_T(t)$ in the presence of a density isomer (upper curve). Lower curve: normal nuclear matter.

Effectively the thermal conductivity also takes into account particle emission - i.e. for example cooling due to pion - and nucleon evaporation. These investigations are being pursued presently by G. Buchwald (1979) in two- and three-dimensional calculations.

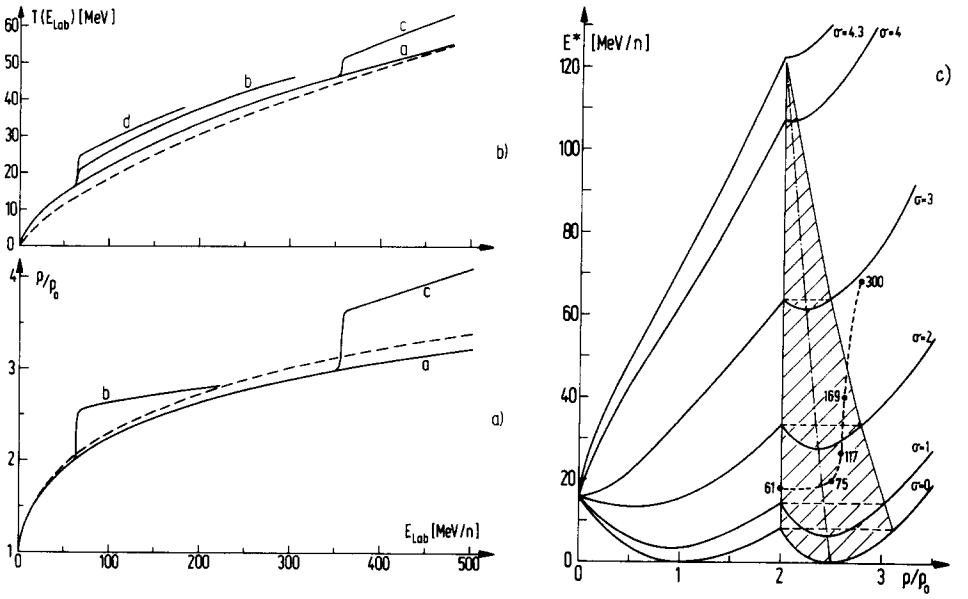

Fig. 23. (a)The central compression ρ/ρ_o increases smoothly with the bombarding energy up to the critical point for the production of a density isomer.Then the system collapses into the abnormal superdense state:the density increases suddenly.Curve a,normal nuclear matter,dashed curve: result of relativistic shock calculation[4,5]; b,density isomer with $\rho_c/\rho_o=2,\rho_1/\rho_o=2.5,B_1=0$; c,density isomer with $\rho_c/\rho_o=3,\rho_1/\rho_o=4,B_1=0$. (b)Similar to Fig. (a) a threshold increase of the excitation function of the mean temperature $T(E_{LAB})$ reflects the presence of a density isomer. This may be used to detect density isomeric states experimentally(see text).Curve a,normal nuclear matter; b,density isomer with $\rho_c/\rho_o=2,\rho_1/\rho_o=2.5,B_o=0$;c,density isomer with $\rho_c/\rho_o=3,\rho_1/\rho_o=4$, $B_1=0$; d,density isomer with $\rho_c/\rho_o=2,\rho_1/\rho_o=2.5,B_1=-10$ MeV. The rate of increase of T may be used to determine the depth B_1 of the secondary minimum. (c)The expansion of the compressed nuclear system approximately follows the curves $E^*(\rho)=E_c(\rho)+E_T(\rho,T)_\sigma$ of constant entropy σ (solid lines).These curves still exhibit the secondary minimum for rather high excitations. The shaded area indicates the region for which "fusion" into metastable abnormal states may be possible (see text). The dot-dashed line gives the position of the respective minima os the isentropic curves. The dots mark the state of strongest compression and excitation obtained numerically for the indicated bombarding energies (in MeV/n). The dots within the shaded area actually represent the "numerical fusion events.

Formation of Abnormal Superdense States

Again we find an important effect of a density isomeric state on the thermodynamical variables like ρ and T. When the critical density ρ_c is reached, only a slightly stronger compression results in the collaps of the central compression region into the abnormal state. This also means that the density now becomes

considerably larger than that calculated with an equation of state without density isomer (Fig. 22a, 23a). As the collision time $\tau_{coll} \approx 10^{-22}$ sec is very small compared to the tunnel time τ_{tunnel} necessary to form the equilibrium phase composition, a Maxwell construction for the van der Walls-type equation of state is meaningless during the fast collision process. As a function of the bombarding energy, the compression increases drastically at the threshold for the production of the density isomer (see Fig. 23). Qualitatively the same effects hold for the thermal excitation energy: When the system collapses into the abnormal superdense state, the temperature increases immediately due to the gain of condensation energy (see Fig. 23b). Contrary to the increase of the density, which experimentally is not directly observable, the increase of the temperature may be used to detect the abnormal state: Analogously to the density (see Fig. 23a), the temperature of the system as a function of the bombarding energy shows a drastic increase at the threshold for the formation of the density isomer (see Fig. 23b). As a consequence of the higher temperature, a threshold increase of the high energy parts of the energy spectra of the emitted fragments as well as the pion production rate will reflect the formation of abnormal superdense nuclear matter. On the other hand, fast emission of highly energetic particles can serve as a cooling mechanism for the abnormal nuclear matter. Such mechanisms are not yet included in our model. Thus the formation of metastable, fused superdense nuclei seems feasible for a range of bombarding energies (see Fig.23c).

During the compression stage, the system becomes thermally excited, i.e. a lot of entropy is produced. However, the system starts to expand from the state of highest compression along curves of constant entropy . These curves will exhibit the potential barrier at ρ_c, although the barrier height and density of the secondary minimum become lower for increasing entropy. Therefore, if the energy of the final compression state is smaller than the corresponding isentropic barrier (analogous to the centrifugal barrier), the system can be trapped within a metastable state, from which it may deexcite into the cold density isomeric state via emission of particles from the nuclear surface. Thus, e.g. for U-U collisions, even the production of (meta) stable collapsed superheavy nuclei, which also have very interesting atomic properties, may be feasible. But also at bombarding energies above the fusion region, where the excessive kinetic and thermal energies lead to the decay of the system, it may still remain rather long within the abnormal phase. We find such a behaviour in our model calculations (see Fig. 23c): For the three bombarding energies E_{LAB} = 75, 117, 169 MeV/n, the state of greatest compression lies within the fusion region. Acutally, we could not find a subsequent decay of the formed abnormal system during the time of the calculation (which was considerably longer than the collision time). On the other hand, for energies at 61 MeV/n (which is still undercritical), and 300 MeV/n respectively, we find that the system dissolves again relatively quickly. This apparent energy window for producing "stable" abnormal matter depends, of course, on the location and shape of the barrier between normal and abnormal nuclear matter. Hence our schematic calculations should only be taken as illustration of the physics to be expected, if the equation of state contains exotic features.

In the next paragraph the collisions of two heavy nuclei are studied in a three-dimensional model. This model does not include viscosity and thermal conductivity, but it allows for the theoretical investigation of the modifications due to the three-dimensional case compared to the schematic results obtained here. It especially leads to a decrease of the achievable compression ρ/ρ_o^{Max} as the matter will strongly be pushed to the sides.

8. THREE DIMENSIONAL CALCULATIONS OF HIGH ENERGY COLLISIONS OF EQUAL NUCLEI

To compare the results of the three-dimensional NFD calculations directly to the

relativistic shock calculations and to the one-dimensional non-relativistic Navier-Stokes results, let us go back to the Euler equations (Stöcker,1979). In the presently discussed hydrodynamical calculation, local heating is neglected. This is reasonable approximation, because one can easily estimate the heat energy produced by the strong shocks from the apparent energy loss in the calculations. Comparing the three-dimensional calculations with earlier one-dimensional calculations with the Navier-Stokes equations, we find that this omission has only a minor influence on the reaction, but in the decompression phase, the internal pressure is too small (the thermal pressure is missing) to ensure the correct expansion velocity. This is not so important for medium energies with moderate thermal excitation but for the higher energies it should be taken into account. The collision of two Zr-nuclei at E_{LAB}=200 and 400 MeV/n was used to investigate the influence of the details of the density isomeric state, which is represented by a parabolic expansion of $E_c(\rho)$ around the secondary minimum (see Fig.4):

$$E_{c_1}(\rho) = \frac{K_1}{18\rho\rho_1}(\rho - \rho_1)^2 \quad \text{for} \quad \rho > \rho_c = 2\rho_o \quad .$$

The influence of the density isomer on the reaction is analogous to the results obtained above.

Let us now investigate the dependence of the formation of density isomers and of the compression rate on the mass of the reacting nuclei and on the parameters of the density isomeric state, respectively. To do this we have calculated the reaction Uranium on Uranium at b = 0 fm and 200 MeV/n with the above equation of state. We find only a slight increase of the maximal compression, but generally the same characteristics as in the Zr case. On the other hand, the dependence of the compression on the nuclear equation of state is significant. Lowering the isomeric compression constant $K_1 = 9\,\rho_1^2 \partial^2 E_c/\partial^2|_{\rho_1}$ from 3000 MeV to 300 MeV is sufficient to increase the compression from 2.88 to 3.41 at E_{LAB} = 200 MeV/n. Using a density isomer with $\rho_c = 3\,\rho_o, \rho_1 = 4\rho_o$, $E_c(\rho_c)$ = +6 MeV, $E_c = (\rho_1)$= -26 MeV results an even much stronger compression,namely ρ/ρ_c = 4.8 for E_{LAB} = 400 MeV/n. We find that the threshold bombarding energy for the formation of a density isomer as characterized in Fig. 4 is located somewhat below 100 MeV/n. This value is considerably higher than the 60 MeV/n obtained in the one-dimensional Navier-Stokes calculations. This is due to the outflow of matter perpendicular to the collision axis. At 200 MeV/n, the critical impact parameter is b = 7±1 fm, corresponding to an isomer formation cross section of

$$\sigma_{DI} = 1540 \pm \begin{matrix} 450 \\ 300 \end{matrix} \text{ mb} \quad .$$

To compare the nuclear density distributions, as obtained with and without density isomer, directly to the one-dimensional results, Fig. 24 shows cuts through the density distribution along the collision axis ($\rho(z)$, left-hand side) and perpendicular to the collision axis ($\rho(y)$, right-hand side) for a head-on collision of two Zr-nuclei at E_{LAB} = 200 MeV/n. The dashed curves show the density distributions at various times obtained with a normal nuclear equation of state (i.e. no secondary minima in $E_c(\rho)$). The full curves show the analogous results (i.e. the same reaction at the same time) calculated with a density isomeric minimum in $E_c(\rho)$ with a barrier of $E_c(\rho_c)$ = - 8 MeV at a critical density $\rho_c = 2\rho_c$, and the density of the abnormal state at $\rho_1 = 2.5\,\rho_o$ with $E_c(\rho_1)$ = -16 MeV (see Fig. 24).

The upper curves show various stages during the compression phase of the reaction. It is clearly seen that the matter approaching the center of momentum along the z-axis during the reaction is pushed out perpendicular to the collision axis, i.e. along the y-axis. The incident longitudinal momentum is transferred into transverse momentum. This will result in the predominant outflow of matter at center of mass angles of about 90°. This prediction of the hydrodynamical model can be tested experimentally (see below).

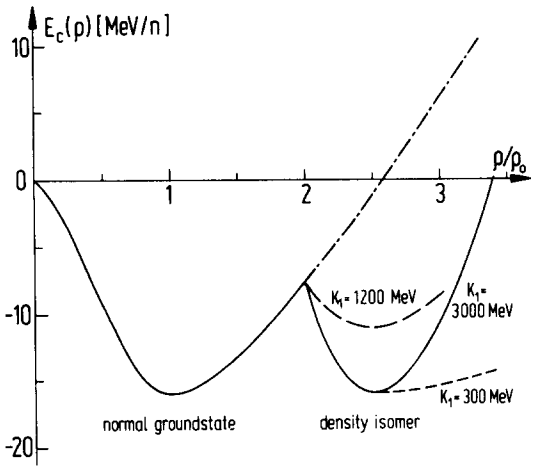

Fig.24 a. The nuclear equation of state used in the three-dimensional calculations shown in Fig.24b.

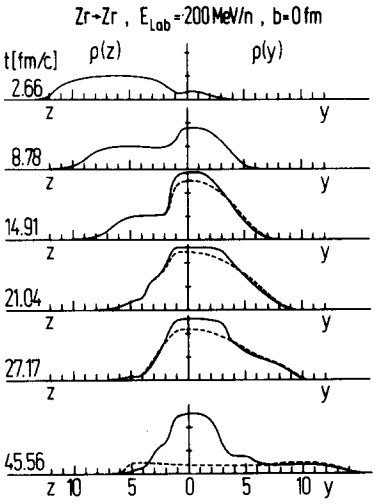

Fig.24 b. The density distributions $\rho(z)$ (left) and $\rho(y)$ (right) of a Zr→Zr head-on collision at E_{LAB}=200 MeV/n resulting from a normal (dashed curves) and density isomeric equation of state (full curves) are shown (see text).The curves are to be reflected around the center of mass(y,z=0) respectively.

The perpendicular outflow is stronger in the case of a normal equation of state, while for the density isomeric case the matter is sucked into the isomer, therefore the internal pressure is smaller, resulting in a less pronounced sidewards flow. This may serve as another possibility to detect abnormal nuclear matter experimentally. In analogy to the previously obtained result, the central compression is larger in the presence of the density isomeric state (see Fig. 24). Yet again the most important difference is the following fusion-like "trapping" of the nuclear matter within the abnormal state. While the formation of the superdense matter seems to be rather similar in the two different cases, the decompressed process differs dramatically (lowest curves): For a normal equation of state there only remains a completely dissolved system with very low nucleon density ($\rho/\rho_o \lesssim 0.4$ at t = 40 fm/c, whereas in the isomeric case at the same time a strongly compressed "fused" density isomer surrounded by a dilute atmosphere can be seen. From the low density regimes mainly small reaction fragments will be emitted, i.e. one can expect that central violent collisions result in events with high multiplicities of the emitted fragments. The density isomer may be viewed as a highly excited object moving with the center of mass velocity. The trapping occurs also when the isomeric ground state is energetically less favourable than the normal ground state. This is due to the isentropic expansion of the matter.

We have mentioned already that the occurrence of shock waves in fast central collisions of equal mass nuclei implies a predominant outflow of matter perpendicular to the collision axis. This effect has been predicted very early (Scheid,1968; 1974;1974a; Baumgardt,1976) and constituted one of the earliest predictions in

nuclear shock waves. A recent experiment of the GSI-Marburg-Berkeley collaboration (Wolf and co-workers,1979; Meyer,1979) seems to present evidence for this sidewards splash in the reaction Ar Ca at 1.05 GeV/n.

They detected π^+ in nearly central collisions and measured the pions transverse momenta and rapidity, which is essentially the forward momentum (see Fig. 25). The pion production itself can be viewed as a trigger for centrality. They predominantly find pions emitted with a forward momentum corresponding to the center of mass velocity of the equal mass nuclei, and a rather large sidewards momentum $p_{/M} \approx 0.5$. The maximum in the contour plots is interpreted as a pion emitting source, moving with $v_{source} \sim 0.5c$ to 90° in the CM-frame. This is just what we expect from our calculations. When the compressed, hot matter flows to 90° in the CM-frame. This is just what we expect from our calculations: When the compressed, hot matter flows to 90° in the CM-frame, during the whole expansion stage fast particles will be emitted. Due to the collective flow of the emitting matter the transverse momentum versus rapidity distribution will show up a maximum at the cm rapidity but at finite $p_\perp$. This effect will be even more pronounced, as the pions from the initial compressed stage can also escape only under 90° in the CM-frame, because of the shadowing effects of the residual projectile and target nuclei, in the forward-backwards hemisphere. As the velocity and temperature of the pion emitting source are time-dependent, no narrow peak but a broad sidewards bump is expected.

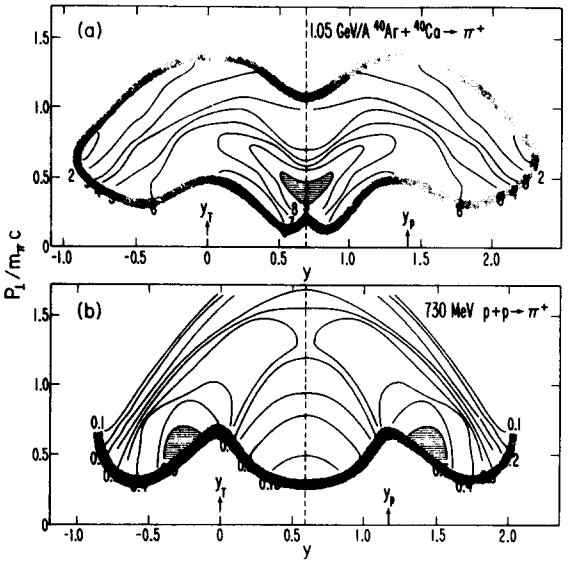

Fig. 25. The rapidity-perpendicular momentum plot of π^+ obtained experimentally in heavy ion collisions shows clearly the sidewards emission of π^+ in contrast to the results for proton-proton collisions where forward-backward emission of π^+ is observed.

From our one-dimensional calculation (see Fig. 19) we can estimate the outflow velocity. During the stage of high compression, the thermal energy is largest - therefore we expect that the thermal pion production occurs mainly in that stage.

For 1 GeV/n and $\rho/\rho_o > 2$, the outflow kinetic energy increases from E_{kin} = 0-100 MeV/n, corresponding to flow velocities $v/c \lesssim 0.5$. To obtain some more detailed information on this subject, we performed a set of three-dimensional calculations for the case studied experimentally. For these high energy collisions the shock heating has been taken into account properly, as it is most important for the expansion stage. This (accounting for convective heat flow) can be done only by working in the center-of-momentum frame, where the energy per nucleon is the same for all nucleons. Then the the thermal pressure and -energy as well as the temperature can be calculated at each point in space from the discrepancy between the initial and instantaneous energy. However, we remark that the energy density and internal energy vary over all space. The use of a non-relativistic model at bombarding energies $E_{LAB} \sim 1$ GeV/n is not too bad when working in the center of momentum system: Here the kinetic energy per nucleon is only 1/4 of that in the lab, i.e. $E_{CM} \sim 250$ MeV/n and $\gamma_{CM} \sim 1.25$, Therefore, the deviations from a relativistic treatment will be on the order of 25%. This seems to be not too bad for these exploratory investigations. The resulting density contour plots for the reaction Ar Ca are depicted in Fig. 26 for various impact parameters at E_{LAB} = 400 MeV/n. Again it is found that for the central collisions a complete desintegration of the projectile and target appears (normal equation of state). The hot compressed matter is squeezed out into 90° in the center of momentum frame.

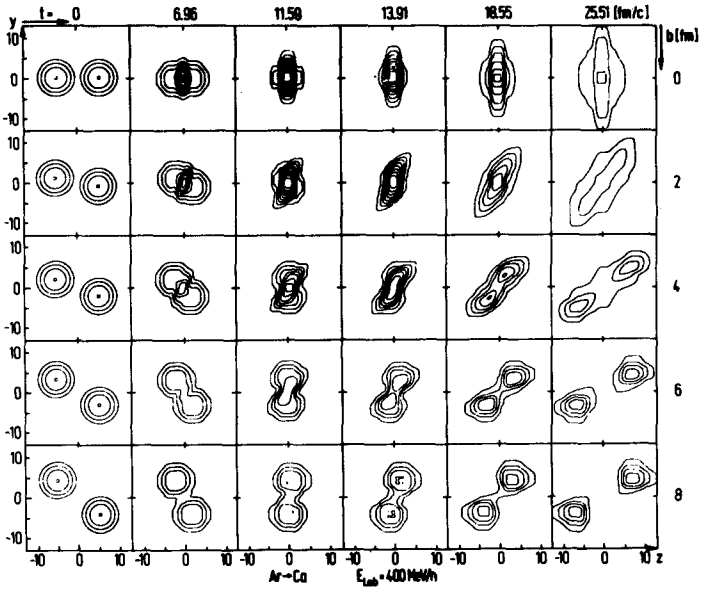

Fig. 26. The density contour plots Ar→Ca are shown at various impact parameters (numbers at the right-hand side) and at various times (indicated on top).

For the more grazing impact parameters the target and projectile are also excited, but they stay rather compact. Therefore we expect that grazing collisions lead to particle evaporation from the target and projectile, which practically maintain their initial velocities. If the impact parameter is lowered, a collective transverse momentum transfer to the whole target and projectile is observed. The nuclei are also much stronger excited - they may not survive the reaction but decay into smaller fragments. For the nearly central collision b = 2 fm, the picture looks like a central collision with a finite rotation energy. One sees that the matter is smashed sidewards with a slight forward-backward asymmetry around 90° in the

center of mass. Also the calculated transverse momentum versus rapidity shows up maxima in the heart-form as is seen in the experiment (Fig. 25). However, as expected, the velocity of the matter (i.e. the pion emitting source) varies continuously in time. For the high temperature stage, where pion production is most probable, then a bump in the transverse momentum distribution appears at

$$p_\perp/_M = 0.1 - 0.4 \quad \text{and} \quad p_{II}/_M = \frac{v_{CM}}{c} \pm 0.2 \quad \text{for } E_{LAB} = 400 \text{ MeV/n}.$$

For 1 GeV/n, qualitatively the same phenomena are found, however, the momentum transfer is larger. The bump is also broader due to the higher excitation energy. For b = 0 collisions we find $p_\perp/_M \approx 0.1 - 0.7$, but a rather narrow $p/_M$ distribution. If the corrections due to relativistic kinematics are accounted for properly - they lower the velocities by ~20% - we find that the velocity of the sidewards squeezed matter is close to the experimentally determined velocity of the pion emitting source.

In conclusion, the recent measurement of a pion emitting source moving with large transverse momentum to 90° in the center of mass system can be viewed as a further indication for a quasi-hydrodynamic behaviour of nuclear matter in high energy heavy ion collisions. However, the model has to be improved in the future to incorporate consistantly the pion emission process in the calculations.

9. MACH SHOCK PHENOMENA AND THE HIGHLY INELASTIC BOUNCE-OFF EFFECT IN COLLISIONS OF SMALL PROJECTILES WITH HEAVY TARGETS

In the violent reactions of small projectile nuclei with heavy targets, the compression effects reflect in somewhat different phenomena than in the collision of equal mass nuclei. For central collisions, the projectile nucleus penetrating into the target is surrounded by target matter - thus we expect to observe the strongly compressed projectile - which is called the head shock - not directly(Stöcker, 1977a). However, compression- and heat waves (the Mach shock) will travel through the target matter, which allows to study the transport phenomena in nuclear matter (see Fig. 27). This was first predicted by Baumgardt (1975) and Hofmann(1974). When the projectile enters the target with hypersonic velocity (the diving phase), strong local compression and heating of the matter near the contact point occurs. When this head shock continues to interpenetrate the target as a projectile-like object with hypersonic velocity, it pushes matter to the side. This initiates a

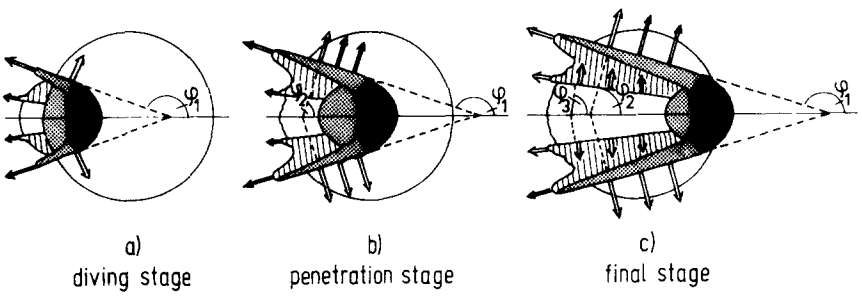

Fig. 27. Various stages of central collision of a light nucleus into a heavier one with the sidewards travelling Mach shock wave are shown schematically.

compression wave which has been called Mach shock wave travelling sidewards through the target matter. This phenomenon allows to study the transport of compressed matter through a region of ground state nuclear matter, namely the residual target nucleus. The nuclear Mach shock wave can be detected experimentally by observing the azimuthally symmetric sidewards emission of matter (predominantly light nuclei) with medium kinetic energy (i.e. significantly higher in energy), much lower than the kinetic energy of the projectile, but different from the evaporation particles. This is discussed below in greater detail. For intermediate impact parameters, the Mach shock phenomenon becomes less pronounced. Here the highly inelastic bounce-off (HIBO) of the projectile from the target is expected to occur; in this process the projectile due to the compression is scattered to the side and is destroyed, transferring a considerable transverse momentum to the residual target nucleus (see the next paragraph).

Recently a series of measurements have been performed at Berkeley and at Dubna (Meyer,1979; Antonenko,1979). They seem to confirm the pioneering experiments of E.Schopper and collaborators (Baumgardt,1975), which have been interpreted earlier as indication for Mach shock waves in relativistic nucleus-nucleus collisions (see later where this is discussed in detail).

Let us now first discuss the more recent experiments from the GSI-Marburg-Berkeley collaboration (Stock,Gutbrod,Sandoval, Poskanzer et al.,1979). They observe in central collisions of Neon on Uranium a strong sideward emission of nuclear matter, when high multiplicity events with a rather azimuthally symmetric fragment distribution are selected. This is just what has been predicted theoretically if the Mach shock phenomenon appears and strongly supports the earlier measurements of Schopper (Baumgardt,1975; Hofmann,1976). Secondly, in the same reaction strongly φ-asymmetric events with a large momentum transfer on a target-like fragment, accompanied by the 180^{o} correlated explosion of a deflected projectile-like object have been detected (Wolf,1979). This obviously must be interpreted as a highly inelastic bounce-off (HIBO) of the projectile from the target. Our model calculations indicate that these phenomena can be used to detect experimentally the impact parameter in these collisions and to deduce the compression rate in such collisions. This bounce-off is quite analogous to what is seen in Fig. 26 for reactions of equal mass nuclei. We will study theoretically collisions of Neon projectiles with Uranium targets. For the non-relativistic cases let us again use the three-dimensional fluid dynamical model where the same nuclear equation of state and potentials as in the last chapter have been used. Again we work in the equal velocity frame, because of two reasons: First, the local shock heating can most easily be computed in all space within this system. Secondly, the computing time is only half of that when working within the lab frame, because the integration time steps can be doubled.

Results for Central Collisions

First let us investigate theoretically with a normal equation of state the collision of the Ne-projectile with an Uranium target at b = 0 (head-on collision) for E_{LAB}=400 MeV/n. Fig. 28 shows a cut through the scattering plane. Snapshots of the collision are depicted in the form of contour plots of the density in the scattering plane. The density increases by 0.04 fm^{-3} from line to line. The outer line represents 0.02 fm^{-3}, i.e. approximately a tenth of the ground state density $\rho_o \approx 0.17$ fm^{-3}. The collision time in fm/c is indicated by the numbers within each plot. The length scale in fm is depicted at the left. Remember that our calculations proceed in the equal velocity frame, therefore the target moves to the left. As the target hits the projectile with hypersonic velocity $V_p \approx 0.46$ c (while $c_s \approx 0.15$ c), a head shock zone is formed during the diving phase of the reaction (t~5-8). This strongly compressed and highly excited projectile-like object continues to interpenetrate the target with supersonic velocity, pushing the matter to the side, thus initiating the formation of a sidewards travelling Mach

shock wave within the target nucleus (t~11-20). The density of the matter within the Mach shock decreases with the distance from the head shock, being always considerably smaller than the head shock density. Due to this effect and due to the deceleration of the projectiles, the Mach shock is curved (not a clear cone as in a Mach sound wave). Because of the additional high temperature within the matter, one expects that the emitted matter (mainly light fragments because of the high thermal excitation) will peak strongly, but not too sharply, to the sides. This peak should be narrower, when only α particles or other larger nuclei are investigated, because they carry most clearly the "collective direction" of the Mach-shock wave: They would be destroyed, if they make a temperature collision. Observing them thus means, that they are not temperature-scattered. There are also other reasons for observing the Mach shock in the α-particle window: The pion condensate - a spin-isospin lattice - is expected to be formed in the Mach shock wave and to break up substantially into α-particles. Also, α-particles are expected to be concentrated within the atmosphere of normal nuclei. Because a shock wave would eject mostly the surface particles, again an α-particle window would be predicted.This narrowing of the sidewards Mach shock peak has been first reported experimentally by selecting mainly α-particles in 4π particle track detectors by Schopper and co-workers(Baumgardt,1975). Indeed, also in the above mentioned experiment of the GSI-Marburg-Berkeley collaboration, the predicted sidewards emission of matter has been observed in an electronic experiment measuring the proton angular distribution. However, the sidewards peak of the emitted protons can be seen only, when "central" events are selected, which are identified with high charged-particle multiplicities and azimuthally symmetric charge distributions.For Ne→U at 400 MeV/n the peak position was found at 60° for $E_p \approx 50$ MeV and at 50° for $E_p \approx 100$ MeV. We calculated the angular distribution of the emitted matter averaging over impact parameters b≤4 fm and - because of better statistics - over the calculated currents during the last 25% of the reaction, where the matter expands

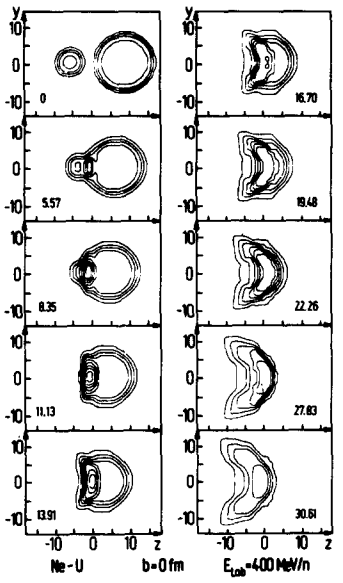

Fig.28. The density contour plots for the collision Ne→U at b=0 fm and E_{LAB}=400 MeV/n as resulting from our three-dimensional calculation.

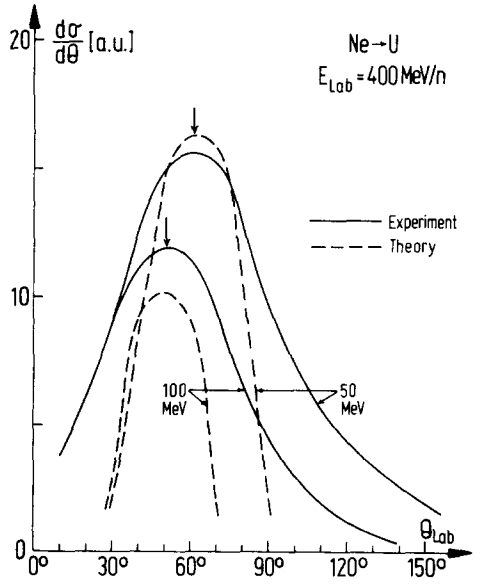

Fig.29. The experimental angular distributions (full curves) are compared to the theoreticall obtained curves (dashed).

and flows apart. Without fitting anything we find peaks in the angular distribution, which are centered at 60° for E_{kin}=50±20 MeV/n and at 50° for E_{kin}=100±10 MeV(see Fig. 29). These are just the same peak positions as found experimentally. In our calculation, for smaller angular bins (±5° instead of ±10°) the peak positions do not change. However, the peaks become rather narrow. The peak is broadened due to the additional thermal smearing, caused by an isotropic Maxwellian distribution of the internal nucleonic velocities. Moreover, not only the peak positions are in good agreement with experiment,but also the relative height of the peaks agree reasonably well. A complete angular distribution for various energies of the observed emission particles in high multiplicity events is shown in Fig.30. It is due to Meyer, Gutbrod, Stock, Sandoval, Poskanzer et al.(Meyer,1979). One can clearly recognize the Mach-shock particles with energies between 10 MeV/n and 2000 MeV/n all peaking around 50°-60° and also the backward directed "diving splash" which is seen for particles with energies around 5-10 MeV/n. The latter is also predicted by fluid dynamics (see Fig. 27) and was already predicted in the very early work by Schopper and co-workers (Baumgardt,1975).

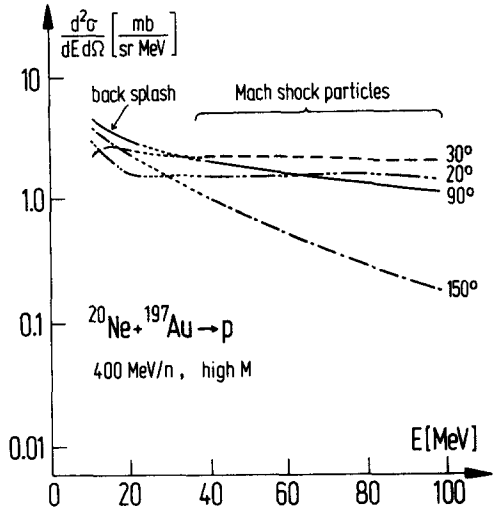

Fig. 30. The experimentally obtained double differential cross section $d^2\sigma/d\Omega dE$ for Ne→Au at 400 MeV/n triggering for the high multiplicities as obtained by Meyer et al. (1979).

The comparison of our theory to the experimental data seems to support the interpretation that compression takes place in high energy heavy ion reaction and that Mach shock waves are formed in central collisions, which can allow for the search of abnormal nuclear matter (see section 10).

Results for Non-Central Collisions

While the central collisions seem to be associated with a total desintegration of target and projectile, in non-central collisions large target- and projectile-like fragments can be observed. We would like to discuss here a new effect occurring in the intermediate impact parameter region, which can be viewed as a highly inelastic

bounce-off (HIBO) of the projectile from the target (Stöcker,1979c). In this process, the projectile is scattered by a compression potential to the side, as is the strongly hit target matter, while a rather large part of the target stays bound. To this heavy target fragment a large transverse momentum is transferred, showing a collective response of the whole fragment to the interaction. This highly inelastic bounce-off can be detected experimentally by measureing a large target fragment with rather large perpendicular momentum in coincidence with many small fragments going into the forward hemisphere, correlated to the target fragment in 180° in the azimuthal angle. The large amount of small, higher energy particles stem from the explosion (nearly complete destruction) of the projectile-like fragment. Fig. 31 shows this bounce-off effect in the Ne U collision at E_{LAB}=400 MeV/n as calculated within our model for three different impact parameters: b = 4,6, and 8 fm. Again, snapshots at various timesteps are taken. One notices that initially, when the target is just hit by the projectile, for the more central b=4 fm collision again a head shock is formed, which additionally also initiates a Mach shock wave in the target. However, as the upper part of projectile and target appear to each other as if they were generally colliding equal nuclei, also a splashing out of matter perpendicular to the collision axis occurs just in analogy to what is seen in the case of a head-on collision of equal nuclei. The bounce-off effect can be viewed as follows: The strong compression potential deflects a considerable part of the projectile to the vacuum. Thus the first group of particles which should experimentally be detected are those deflected fast light fragments (heavy fragments will not survive the high excitation energy). The second group of particles will stem from the compressed direct reaction zone, which will also explode. Thirdly, a rather large residual target fragment, which was not centrally hit, and therefore is not strongly enough disturbed for total desintegration, can survive the reaction. It can get rid off its internal excitation by evaporating off particles. However, during the reaction a considerable amount of transverse momentum is transferred to the whole target-like fragment, while most of the longitudinal momentum is transferred to the exploding direct reaction -(compression) zone, and partly is also carried away by the sidewards deflected residual projectile-like fragment.

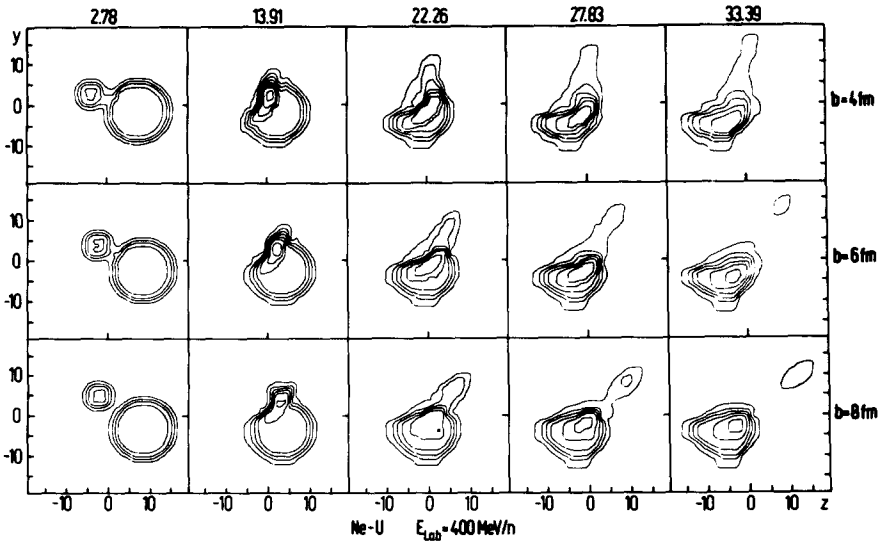

Fig. 31. The density contour plot of the reaction Ne→U at 400 MeV/n for intermediate impact parameters.

For b=6 and 8 fm qualitatively the same picture holds, however, the direct interaction region becomes less compressed with increasing impact parameters, and therefore the interaction between projectile and target is less pronounced (see also Table 1).
The head- and Mach shock become less intense at b=6 fm and can no longer be seen clearly at b=8 fm. A very important feature of the more grazing collision is the change of the scattering angle of the projectile-like fragment to more forward angles with increasing impact parameter (see Fig. 31). It can be viewed as the less pronounced repulsion from a smaller compression potential. We now will show that the dependence of the scattering angle on the impact parameter is of great importance for further analysis of high energy nuclear reaction data, as it can serve as an unique tool to determine the impact parameter of each collision experimentally.

TABLE 1

	b[fm]	0	2	4	6	8
a)	$\langle M_c \rangle^{E_{kin}>30\ MeV}$ (b) :	37	32	27	21	16
b)	$(\rho/\rho_o)^{max}$ (b) :	2.06	2.02	1.90	1.72	1.34
c)	T^{max}[MeV] (b) :	44	44	44	42	40

The dependence of the mean multiplicity $\langle M_c \rangle$ of high energetic particles, the maximum compression and the maximum temperature on the impact parameter in Ne→U collisions at 400 MeV/n as obtained in the three-dimensional calculations.

As the rate of compression in a reaction does also depend strongly on the impact parameter, the above proposed experiment may be used to determine indirectly the rate of compression achieved in fast nuclear reactions. Therefore, similarly to the Coulomb deflection trajectory used to measure the impact parameter in low energy nucleus collision the measurement of the bounce-off effect can be used for impact parameter measurements in high energy nuclear collisions. To make our discussion more quantative, we define the characteristic variables of the "projectile-like fragment" and "target-like fragment" as the variables at the respective region of maximal density and determine the momenta, energy loss and deflection angle in a late stage of the collision, when the nuclear fragments have split again and thus the investigated variables stay constant in time. The results are plotted in Fig. 32 for the different impact parameters: Fig. 32a shows the dependence of the deflection angle of the projectile-like fragment on the impact parameter b. One notices the increase of the deflection angle ϑ_{LAB}^{defl} with increasing centrality. However, it does not look at all as like elastic scattering of hard spheres, but must be viewed as a highly inelastic reaction with strong mutual interpenetration of projectile and target connected with strong compression and thermalization effects. The diving depth of the projectile into the target can be evaluated approximately from the scattering ange by calculating the effective scattering radius

$$R_{eff} = \frac{b}{\sin\frac{\pi - \vartheta_{LAB}^{defl}}{2}} \tag{10}$$

of the scattering of a particle by a hard sphere from the scattering angle ϑ_{LAB}.

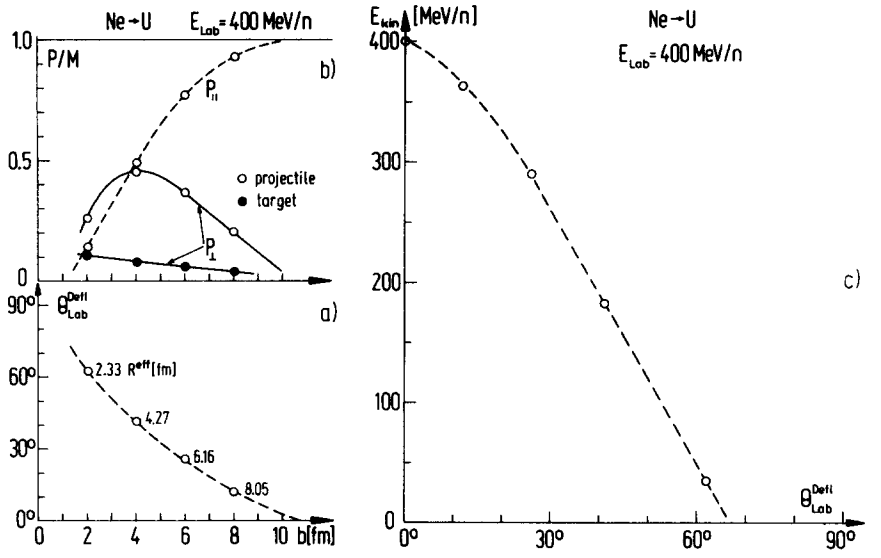

Fig.32. For the collision Ne U at 400 MeV/n we show (a) the dependence of the deflection angle Θ_{LAB} of the projectile-like fragment on the impact parameter b. (c) The forward momentum loss (dashed curve) and sidewards momentum gain (full curve) of the projectile-like fragment (open dots) with decreasing impact parameter and the transverse momentum transfer to the target (full dots). (c) The theoretically obtained deflection function Θ_{LAB} (E_{kin}) is shown.

The numbers in Fig.32a give the effective scattering radius R_{eff} and show that the diving depth d(b) is approximately given by

$$d(b) \approx (R_T - b) \quad . \tag{11}$$

By measuring Θ^{defl}_{LAB} one may therefore also deduce the interpenetration depth for distinct reactions. The measurement of the deflection angle of the projectile-like fragment, however, can not simply be detected, as the highly excited fragment explodes. Thus one has to measure in coincidence the angles and momenta of all explosion products of thes projectile-like fragment to determine its center-of-mass values. The longitudinal momentum p of the projectile-like fragment is another quantity of interest (see Fig. 32b)): p decreases strongly with increasing centrality and for rather central collision it is only of the order of 10% of the initial momentum. The forward momentum is distributed over many particles and is carried away by the explosion products also of the compressed zone, in which the projectile- and target matter are mixed up and strongly excited. The transverse momentum of the projectile is increasing strongly when b goes from 8 to 6 and 4 fm. It decreases again for b = 2 fm - this is due to the practically complete energy transfer ("sticking") to the dense and hot compression zone (head shock) in the case of nearly central collisions. Actually, the transverse momentum $p_\perp/_M$ of the residual target-like fragment is considerably smaller than $p_\perp/_M$ of the projectile, as the residual target still has a rather large mass compared to the rest of the projectile As the dilute nuclear matter of the direct reaction region expands and still connects the projectile- and target-like fragments, we cannot determine

the mass of the residual target, the only conclusion possible in the moment is that the mass decreases with increasing centrality and is always much smaller than the original target mass. For a more detailed information also the evaporation of particles has to be included in the calculation. It is important to point out that the large momentum transfer on the whole heavy fragment implies a collective response of the whole fragment to the compression potential, which acts between the bounce-off projectile and the target. Therefore, the impact parameter dependence of the transverse momentum transfer is an important information on the compression phenomena. Our theoretically obtained values $0.03 \lesssim p_\perp/_M \lesssim 0.1$ are in good agreement with the recent data of the GSI-Marburg-Berkeley collaboration (Meyer,1979). They measured strongly asymmetric events with 180° azimuthal correlation in the scattering plane; for various systems they observe on one side many fast (E_{kin}> 30 MeV/n) light particles and, on the other side, a heavy target (e.g. Z=26) at 90° in the lab (i.e. with small forward momentum) with transverse momenta $P_\perp/_M$ (e.g. they found values of $p_\perp/_M \approx 0.036$, which are in the same region as our results).

In our calculations we obtain practically no longitudinal momentum transfer to the target-like fragment - the same as is observed experimentally. The calculated multiplicities of charges with E_{kin}>30 MeV/n depend on the impact parameter (see Table 1). In these experiments it is found that the production of such target-like fragments is predominantly seen for rather high charged particle multiplicities $\langle M_c \rangle \sim 10\text{-}20$ within E_{kin}>30 MeV/n. This in our model corresponds to impact parameter b~6-8 fm, when one takes into account the formation of composite particle which we did not discriminate in our $\langle M_c \rangle$ determination from single nucleon. Fig. 32c shows the deflection function of the Neon-like fragment at 400 MeV/n. The kinetic energy loss is larger than 90% of E_{LAB} for $\varphi \lesssim 60°$, which corresponds to a rather central collision (b<2 fm), but already for $\Theta_{LAB} \approx 30°$ the kinetic energy loss of the projectile-like fragment is of the order of 25%. Contrary to the elastic Coulomb scattering in low energy heavy ion collisions, all scattering processes in the high energy region with impact parameters $b<R_T$ lead to highly inelastic events. By detailed coincidence measurements of these highly inelastic bounce-off effects it will be possible in the future to measure the impact parameter also for collisions at relativistic energies. The various variables, which have to be determined experimentally to deduce the impact parameter, are:
(a) The charged particle multiplicity of fast particles which increases with the centrality. (b) The azimuthal symmetry of the events - symmetry should only appear for very small impact parameters $b \lesssim 2$ fm. (c) The azimuthal asymmetry with 180° correlation in the intermediate impact parameter region. The correlation between the target-like fragment and the exploding projectile-like fragment going hand in hand with the collective response (large perpendicular momentum transfer) of the fragments, the longitudinal momentum loss and the total kinetic energy loss of the projectile-like fragment and the deflection angle of the center of mass of the fast, sidewards pushed particles. From the measuremen of these quantities we can deduce the degree of violence and the diving depth in the reactions, from which not only the impact parameter, but also the compression rates and shock heating can be estimated by comparison with the theory (see our Table 1).
The compression rates obtained are low compared to one-dimensional shock calculations, which at 400 MeV/n yield $\rho/\rho_0^{max} \approx 3.4$. This is largely due to our three-dimensional tratment; the matter pushed to the side can freely expand into the vacuum. To a certain extent this also comes from the smallness of the projectile, which dissolves before the stage of largest compression is reached. For example in U-U collisions, one can reach a rather stationaly stage of constant compression in our calculations. The width of the shock fronts we obtain is of the order 1.5-2 fm, but it depends on the reaction considered. This is more realistic than the infinitely sharp shock fronts used in the simpler model calculations and in a different fluid dynamical approach.

Conclusions

One can split violent collisions of light nuclei with heavy targets into two types, namely nearly central collisions, which exhibit the strong compression phenomena most clearly by the sidewards moving Mach shock wave and very high azimuthally asymmetric fragment distribution with strong sidewards peaks, and the intermediate impact parameter collisions leading to the highly inelastic bounce-off, where the compressed matter acts in analogy to a repulsive spring which releases strong collective transverse momentum transfer. In these 180° correlated events one can learn from the deflection angle and momentum transfer and -loss about the impact parameter and therefore about the compression phenomena in non-central collisions of fast heavy ions. We finally mention, that the results on the deflection function and impact parameter do not depend very sensitively on the equation of state (i.e. compression constant K) used, as long as the nuclear equation of state is normal. If it contains exotic features like density isomers, we expect modifications of the above resulty and even signatures for isomers in the deflection function. Such calculations are presently carried out.

High Density Nuclear Mach Shock Waves and the Search for Density Isomers in Relativistic Collisions

As the Mach shock experiments have not only been carried out at the nonrelativistic energies, but experimental data have been obtained at $E_{LAB} = 4.2$ GeV/n as available in Dubna, we now have to use a relativistic model for interpreting the fast nuclear collisions. We will here investigate the dynamics of a relativistic heavy ion collision in terms of a simplified hydrodynamical model, using a parametrization of the Mach shock geometry similar to the results found in the nonrelativistic calculation. This model allows to study the influence of the nuclear equation of state using the relativistic shock equations. The geometric, thermodynamic- and kinematic variables and their time evolution as obtained in the more schematic calculations are used to yield the mean values of the mentioned variables and of the angular- and energy distribution of the reaction fragments.
In Fig. 33 the typical time evolution as resulting from the calculation is shown. It looks quite similar to those obtained from the full non-relativistic calculations. The calculations are carried out in the lab frame. Mainly three different phases of evolution during the collision can be seen (Baumgardt, 1975).

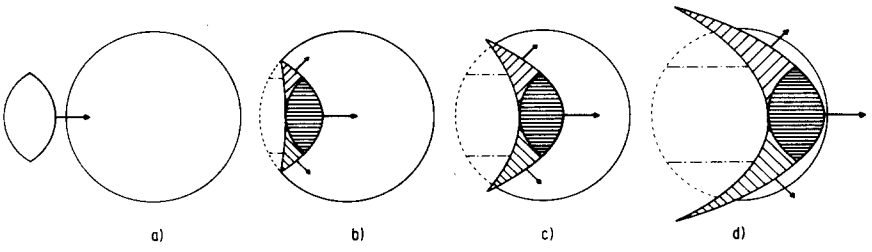

Fig. 33. The geomatry of the relativistic Mach shock model is shown for various time steps.

The diving phase: The kinematically contracted projectile enters the target, becomes highly compressed and excited. In the diving process a splashing wave should lead to backward emission of matter.

The penetrating stage: The projectile interpenetrates the target, pushing matter to the side; thus initiating the sidewards travelling strongly compressed Mach shock wave.

The evaporating phase: The projectile- and Mach shock matter leaves the residual target, which now evaporates, while projectile and Mach shock explode because of their very high excitation energies, which correspond to temperatures from 20-60 MeV.

The explosion of the head shock wave which contains at the end of the collision more than double the nucleons of the incoming projectile, is what has been named recently the explosion of the "nuclear fireball" which has been used to explain angular- and energy distributions in non-central high energy heavy ion collisions. It may be possible, that the strongly compressed and highly excited projectile explodes inside the target during the interpenetrating state. This will lead to superstars with enormous multiplicities. In this case the Mach angle will be washed out and cannot be seen. This will be taken into account in a further calculation. As mentioned earlier, the nucleus-nucleus encounters are quantum mechanical processes with corresponding probability distributions. A classical hydrodynamical calculation can therefore be viewed at best as a calculation of the mean values of the quantum mechanical system in the sense of Ehrenfest's theorem. Superimposed to that are always the quantum fluctuations. They lead under the same initial conditions to events with sticking of the projectile and its explosion (superstars), to events with a penetrating superstar and a creation of a Mach shock wave and also to events where the projectile is practically little disturbed by the target (semi-transparency). It is a formidable experimental task to discriminate between these events by making e.g. the proper star-selections.
To restrict the number of degrees of freedom, we parametrize the compression zone by two paraboloids, $z = a_1 r^2 + z_1$, $z = a_2 r^2 + z_2$, which describe the shock front and the backside of the compression zone respectively. The undisturbed part of the target nucleus is described by the part of a spheroid of radius R up to the shock front (paraboloid 1), while the residual nucleus is described by a spheroid up to the backside of the compression zone (paraboloid 2) with a drilled hole of radius R_p in it. The residual nucleus has not yet been incorporated in the present calculations. The projectile (head shock wave) is divided from the Mach shock zone by a third paraboloid $z = -a_1 r^2 + z_2$ (see Fig. [33]). Thus the geometry of the system is determined by four variables: a_1, a_2, z_1, z_2. The dynamical variables (energy density, momentum, pressure, temperature, density) are obtained by assuming homogeneous density-, velocity-, and temperature fields in each compression region. Thus for the sake of simplicity we concentrate on the mean values of the physical observables in the different regions as a function of time. The shock equations yield an unique relation between energy, pressure, temperature, velocities, and the rest density in the compression zone. Using these, we can describe the stage of the system by the four geometrical variables and the density in the Mach- and head shock region. To describe the evolution of the system in time, we need six differential equations for these six variables. These equations are obtained by the conditions that the surface points on the paraboloid have to fulfill the shock equations and that total baryon number A and total energy E are conserved. One has to take into account the correct Lorentz-transformations for the various quantities (density,energy,...) in the different regions.The time evolution of the physical quantities is obtained by simultaneous numerical integration of the six differential equations in time-steps of Δt=0.1 fm/c,which is sufficiently exact to ensure energy- and baryon number conservation better than one percent.

Results of the Schematic Mach-Shock Calculations

The head- and the Mach-shock densities ρ_1 and ρ_2 as a function of time are shown in Fig. 34 for various energies: In the beginning, the projectile is strongly compressed, but this compression is substantially decreased later on. The Mach shock density ρ_2 is about $2\rho_0$ below the Mach shock density ρ_1. The mean compression in the head- and Mach shock (each at t=5 fm/c) is shown in Fig. 35a as function of the bombarding energy. The mean kinetic energy $E_{kin} = ((1-v_t^2)^{-1/2}-1)\ W_o$ of the emitted particles (Fig. 35b) after the collision is smaller than 200 MeV/n for Mach shock particles up to bombarding energies of 5 GeV/n, while it is larger than this experimentally important threshold for the projectile (head shock) at high energies. The temperature in head- and Mach shock just after the collision is shown in Fig. 35c. The fragments from projectile, Mach shock wave and the evaporation residues fall within angular domains relative to the beam axis as shown in Fig. 36.

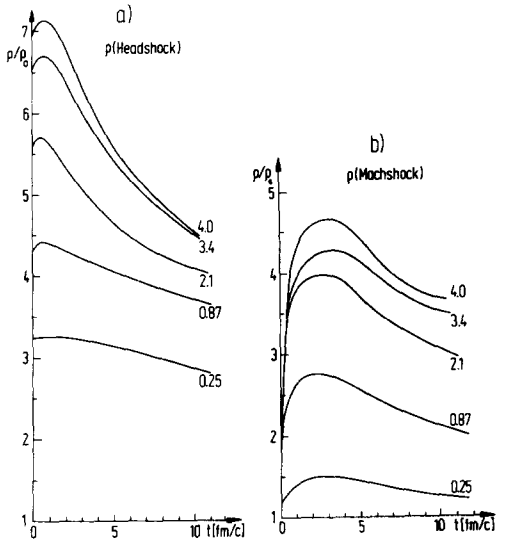

Fig.34. The evoluton of the high densities in the head shock and Mach shock as a function of time.

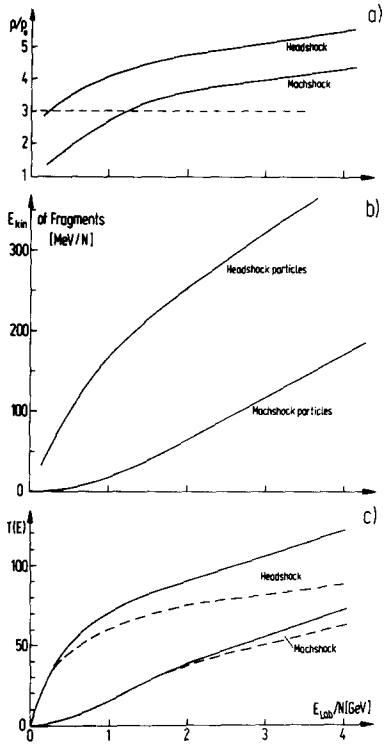

Fig. 35. The density a)kinetic energy of fragments b) and temperature c) of the various compression zones as a function of the incident energy.

As the mean head shock densities are approximately equal to those calculated within the one-dimensional model, we can make use of the latter model to yield the pion production rate, when we take care of the result, that the number of head shock particles is about $2A_p$. The Mach shock angle φ is depicted as a function of lab-energy in Fig. 37. It smoothly decreases from about 60 degrees at 0.1 GeV/n to 35 degrees at 4 GeV/n for a normal equation of state. It is smeared out very much because of the temperature in the Mach shock and because of the curvature of the "Mach-"cone". The explosion of the highly excited head shock causes strong emission of fast particles into forward

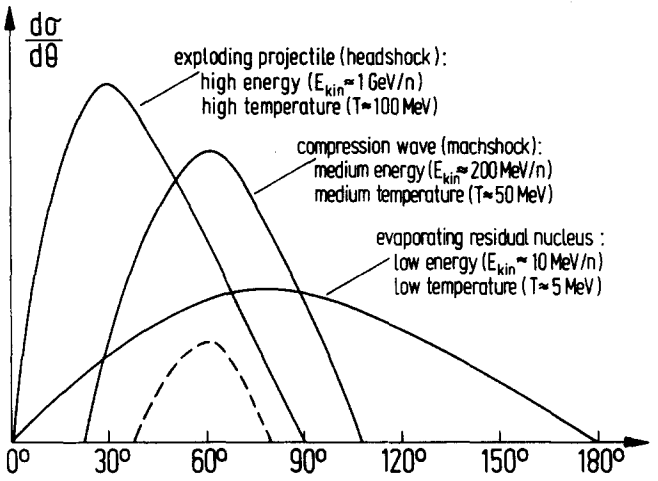

Fig. 36. The fragments of the head- and Mach shock fall into the indicated angular domains. The angular distribution of the evaporation residues is also shown.

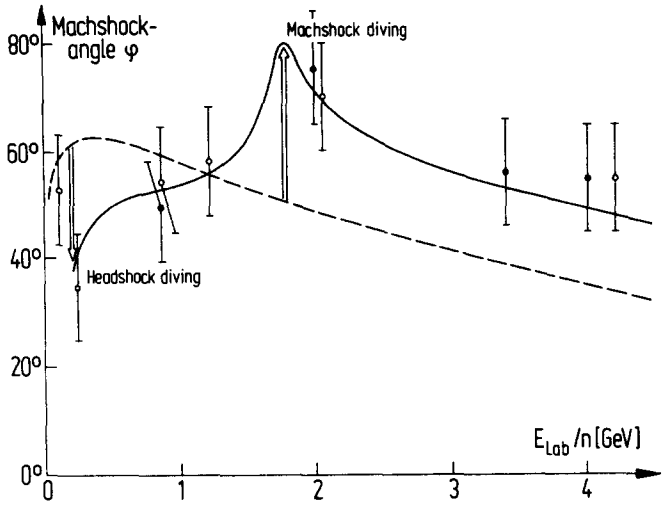

Fig. 37. The Mach-angle φ in dependence of the projectile energy for a normal equation of state (---) and for an equation of state with a density isomer (———).

directions, which may hinder the visibility of the Mach shock peak at small bombarding energies. The energy spectra of the exploding projectiles (head shock) drawn in Fig. 38 were calculated by relativistic addition of the flow velocity and the mean thermal velocity in the head shock after the collision, taking into account the isotropic decay cross section in the rest system of the projectile.

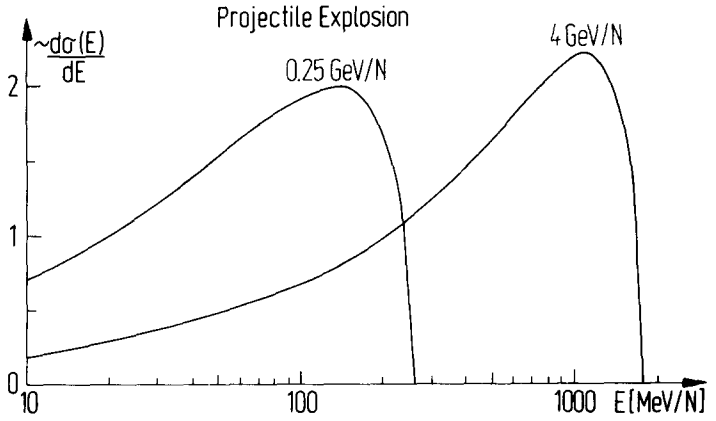

Fig. 38. Energy spectra of exploding projectiles for two different incident energies.

The Influence of a Density Isomer on Mach Shock Waves

If we schematically assume a density isomer at $\rho/\rho_0 \lesssim 3$, the above picture applies only below $E_{LAB} \approx 0.2$ GeV/n, as then the projectile density reaches the phase transition region, i.e. the region of negative pressure ($p<0$). (See Figs. 39,40). The projectile collapses into the density isomeric state. Thus the"quasi-stable nuclear crystal" can move with rather small dispersion through the surrounding normal nuclear fluid. One may thing of a piece of "nuclear ice" which moves through "nuclear water" - this is important for the appearance of the Mach shock wave, since a water droplet dumping into water produces too high friction and therefore soon damps out the collective motion. This, in fact, can to some extent be seen in the full hydrodynamic calculation (see last section).
As during the phase transition the head shock velocity becomes small, the Mach shock angle φ substantially decreases in this energy region, since the Mach shock moves faster than the collapsing head shock during this time period. The crystallization of the projectile causes a much more pronounced Mach shock peak at higher energy, because the projectile moves with much less friction through the target. At bombarding energies of about 1.5 GeV/n the Mach shock density appraches the critical region: Now the Mach shock matter collapses into the density isomeric state and the Mach shock velocity becomes small, so that the Mach angle now will be substantially increased (see Figs. 37 and 39). It will also be broadened out due to the rapid change in Mach shock velocity within a small density regime. At even higher bombarding energies, the Mach angle shall decrease again as both v_{HS} and v_{MS} tend to the light velocity c at very high densities, so that $\varphi \to 0$ for very high energies. One also may think that higher phase transitions do occur, which may again produce such a characteristic dependence of the Mach angle φ on the bombarding energy.

Comparison of the Calculations with the Experimental Observations

High Density Nuclear Mach Shock Waves (HDNMSW) should be observable in central high energy collisions of light projectiles with heavy targets. The pioneering experiments of Schopper et al. (Baumgardt,1975) supplemented by the theory, have

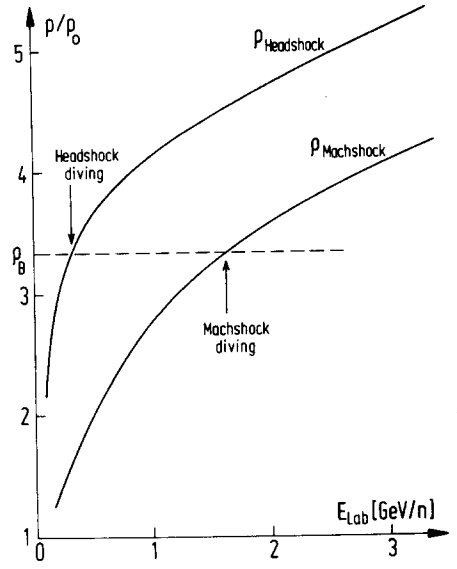

Fig.39. The diving of head shock and Mach shock into a possible second minimum of the equation of state. The head- and Mach shock densities as a function of projectile energy. ρ_B indicates the position of the assumed 2nd minimum in $E_c(\rho)$.

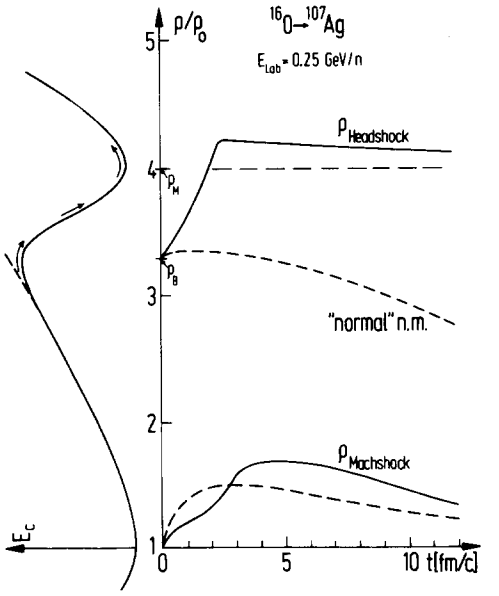

Fig. 40. The time behaviour of head- and Mach shock densities for normal (---) and isomeric nuclear matter (——). Along the ordinate the energy density $E_c(\rho)$ is demonstrated.

set the stage for the criteria to discriminate the Mach shock events from others: 1) In azimuthally symmetric central collisions, which can be identified by very high multiplicities and azimuthally symmetric distributions of the reaction fragments, e.g. by many prong stars in AgCl-detectors or emulsions, a preferential emission angle must be observed. 2) The kinetic energy of these particles will be smaller than 200 MeV/n. It may be decreased to even lower values, if the Mach shock density is in the secondary minimum. 3) The Mach shock peak and the decay of the head shock should predeminantly be seen in the α-particle (or other complex nuclei) channel for three reasons: (a) A pion condensate with a structure of a spin-isospin lattice preferentially decays into nucleons and α-particles as smallest lattice cells. The former can hardly be distinguished from evaporation particles, but the complex fragments can. (b) When the Mach shock wave approaches the nuclear surface, it kicks out the α-particles contained enhanced in the nuclear surface. (c) During the individual collisions of the constituent particles in the high temperature zone of the Mach shock, mainly those α-particles (and heavier clusters) survive, which have not undergone a temperature scattering. Thus the mach angle is conserved by those clusters, while scattered and unscattered nucleons cannot be distinguished. 4) One should find fast pions emitted by highly excited nuclear matter. The occurrence of pion condensation should also lead to a large enhancement of the pion production cross section. 5) Simultaneously to the medium energy sidewards Mach shock peak, a broad high energetic forward peak at $\Theta \sim 40^\circ$, stemming from the exploding head shock, will be seen. It may consist of protons and pions mainly because of the extremely high temperatures in the head shock. (see Fig. 38). The head shock particles are - in

the mean - of energy and can thus be (partly) discriminated from the Mach shock particles. 6) A nearly isotropic distribution in the lab frame may stem from the residual nucleus with small temperatures and kinetic energies.

In the presence of a density isomer the Mach shock peak should be more clearly pronounced and also should have the above predicted dependence on energy. The experimental data of Schopper et al. (Schopper,1979) which fulfill the above criteria on centrality, energy- and α-particle windows, show a peak in the angular distributions of the reaction fragments. The systematic shift of the preferential angle with energy can be interpreted in comparison with our calculations as indication for a phase transition in dense nuclear matter at $\rho/\rho_o \approx 3\text{-}5$ (see Figs.37 and 41 and figure caption).
Deviations in the prong-angular distribution of multiprong stars have also been seen by the Heckman-group (see Fig. 42). These deviations agree with the peaks seen by Schopper et al. and thus supplement the Mach-shock picture. Also the previously discussed angular distributions obtained by Gutbrod, Stock, Poskanzer et al. (see Figs. 29 and 43) show the peak in the same position as those of Schopper.

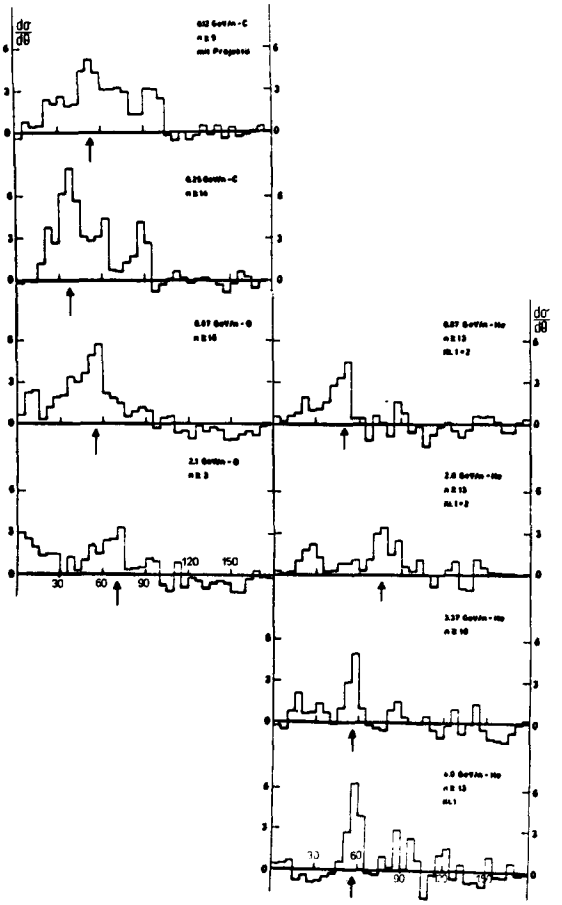

Fig. 41. Angular distribution of prongs for large stars at various energies (after Schopper et al.,1979). The evaporation background had been subtracted. The systematic variation of the peaks can be recognized.

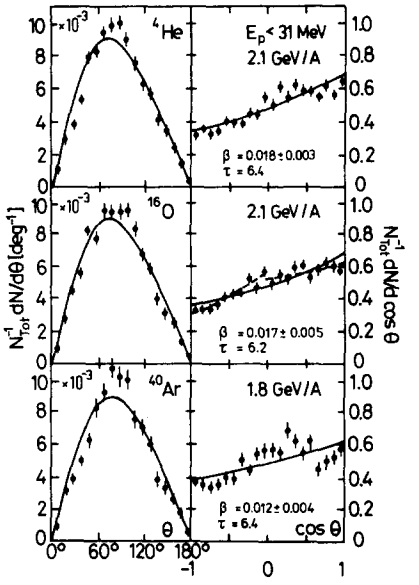

Fig. 42. The angular distribution of emitted particles in the emulsion experiments of Heckman and co-workers.

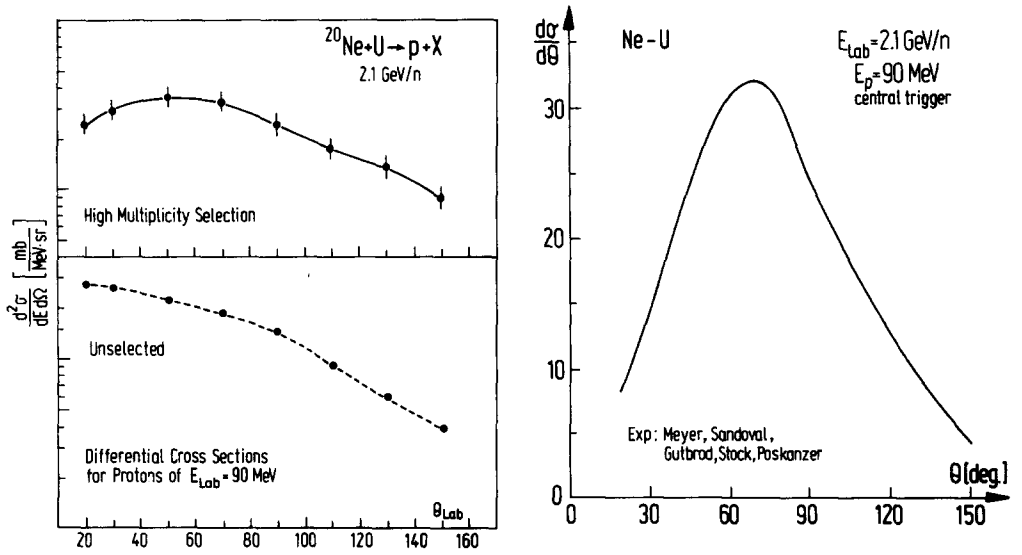

Fig. 43. The angular distribution of protons of 90 MeV lab energy resulting from the collisions of Neon on Uranium at 2.1 GeV/n (left: $d\sigma/d\Omega$, right: $d\sigma/d\,\Theta$).
The sidewards peak is only seen with high multiplicity selection (i.e. central trigger)

Recently, both Heckman and Schopper have measured the angular distributions of only α-particles coming out of multiple prong stars in emulsion. As was theoretically expected, the α-particle distribution shows the Mach-shock peak much clearer. Also the rapidity plots of the Gutbrod-Stock-Poskanzer-group for various clusters (see Fig. 44) seem to indicate that the heavier particles (e.g. the α-particles) stem from a source of intermediate velocity (the collective Mach shock wave). It is this completion of the picture as well as the additional observation of Schopper (1979) and Baumgardt (private communication) that the velocity of the Mach-shock particles is significantly faster than the velocity of the background particles, which strengthens our confidence in the validity of the Mach-shock model. We predict, that the observation of angular distributions of big clusters out of azimuthally symmetric high multiplicity events will yield well recognizable peaks (Mach shock emission) whose dependence on energy will give us most valuable information about the gross features of the nuclear equation of state.

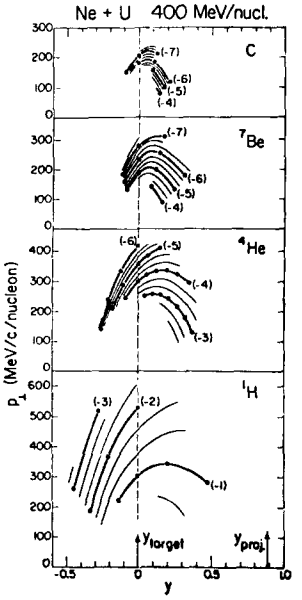

Fig.44. Rapidity plot of the heavier fragments measured by the GSI-LBL-collaboration show emission from medium velocity source.

10. STRONG BOUND PION STATES

In this section we shortly mention a purely speculative phenomenological idea: From the usual description of the pion nucleon interaction by a pseudo-scalar coupling

$$L_{\pi N} = - ig \bar{\psi} \gamma_5 \tau \Psi \vec{\phi}$$

where the pion field couples to the pseudo current

$$\gamma^{\mu}_{5i} = \bar{\psi} \gamma_5 \tau_i \Psi$$

one might expect that for high nuclear densities $\bar{\Psi}\gamma^{o}\Psi$ this interaction becomes very strong. Because of the very non-linear interaction between pions and nuclear matter, one does at present know very little about quantitative aspects at high nuclear density. For the low nuclear densities one knows that the pion-nucleon interaction is rather well described by the Kisslinger (Kisslinger,1955) potential. Ericson and Myrer (Ericson,1978) and others have shown that indeed for heavy nuclei (A>200) the Kisslinger potential may lead to bound pion states in the nucleus,the binding energy of the pion increasing with the nuclear density. This is shown qualitatively in Fig.45 . However, the Kisslinger potential looses its validity at such high densities. Therefore it cannot be definitely concluded that the gap between the π^{+}- and π^{-}-states will actually approach zero for some critical density ρ_c, as suggested by the figure. For instance a strong repulsive interaction at high pion density (e.g. a ϕ^4 term in the π-Lagrangian) may prevent the two states shown in the figure from approaching each other. Though very little is known about strongly bound pionic states in high density nuclear matter. Such states, eventually leading to "spontaneous" π^{+}-π^{-}-production i.e. without loss of energy should indeed by an exciting phenomenon if they exist.

Let us - phenomenologically - assume that strongly bound pion states exist in nuclear matter and ask how such states would reveal themselves in relativistic heavy ion collisions. In some test calculations we assumed that the strong collective nuclear force in highly dense nuclear matter leads to a strongly bound pion state with a small effective pionic mass ($m_\pi^{eff} << m_\pi$), which is supposed to arise from the repulsive - interaction. We found that, owing to the strongly bound pionic state the temperature in high energy heavy ion collisions will be reduced substantially at high densities $\rho/\rho_o \gtrsim 2$ (see Fig. 45). A lot of pions are created in this strongly bound state of rather small energy, thus using up a large amount of the thermal energy of the system. This can lead to a drastic strong cooling even at rather small bombarding energies: These low energetic pionic states can be populated very massively already at relatively low temperature. The sudden reduction of the temperature above the critical bombarding energy necessary for the formation of such a strongly bound state may be detected experimentally as the

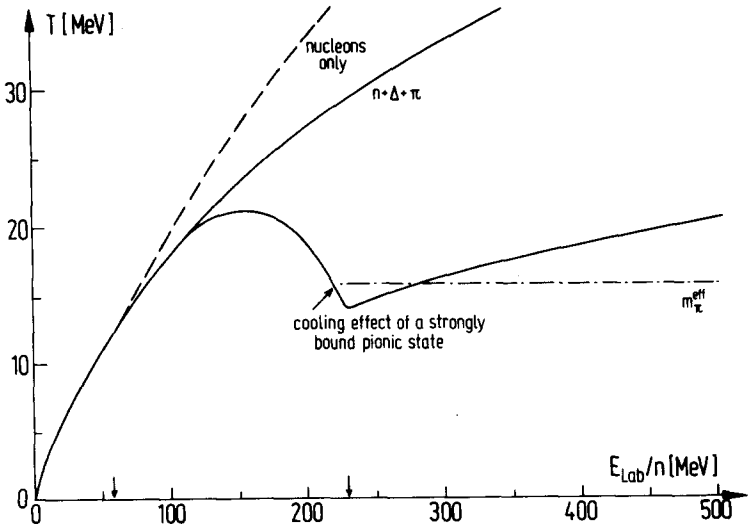

Fig. 45. The presence of a strongly bound pionic state would strongly cool the reaction zone in high energy heavy ion collisions above the critical energy.

evaporation spectra of the reaction products and the mean pion multiplicity strongly depend on the temperature of the compression zone. The pion production rate will be changed additionally because of the following processes: There will be less direct production of free pions as calculated above. However, two step processes, e.g. the excitation of pions from the bound state into the continuum, become important. Also the expansion of the compression zone after the reaction makes the production of free pions, which were originally created in a bound state, feasible.This is so, because of the "adiabatic" extraction of the pions (similar to electron-hole production in intermediate superheavy quasi-molecules) when approaching the upper continuum for smaller densities. Such a process may also lead to a decrease of the limiting temperature in central high energy nuclear collisions.

11. THE LIMITING TEMPERATURE - THE HADRONIC MASS SPECTRUM

Another important question, which can be raised in connection with high energy nuclear collisions is the search for a "limiting" temperature, as suggested by Hagedorn (1965) to occur in a single n-n collision, and suggested for nucleus-nucleus collisions by us (Scheid,1974; Greiner,1975). In the experimentally determined hadronic mass spectrum one notices a fast (actually nearly exponential) increase of the number of particles (resonances, mesons) with the mass of the particles. Presently, because of the limited accelerator capacities, the particle spectrum is practically only known for masses $m \lesssim 3$ GeV. However, if the hadronic mass spectrum is assumed to increase exponentially for all masses(which is a consequence of the bootstrap equations) there should exist an upper bound to the temperature which can be reached in high energy particle collisions. This so-called "limiting temperature" T^{Max} originates physically from the fact that hadronic matter with rising thermal excitation prefers to create particles of increasing mass (see Fig. 46). So, instead of increasing the temperature, higher excitation energy

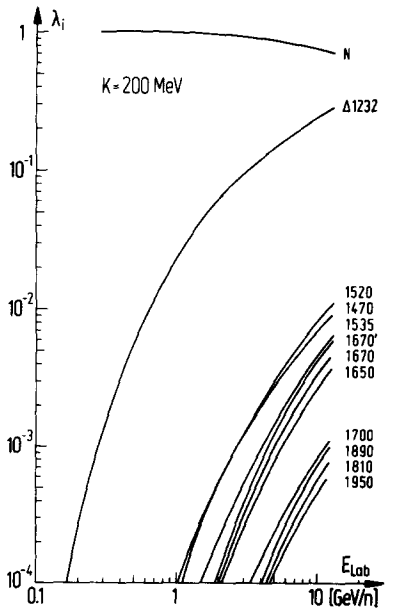

Fig. 46. The probability λ_i for the excitation of various resonances as calculated in the shock model is shown as function of the bombarding energy.

is transformed into mass of heavy particles. This can be seen clearly for the case of nuclear collisions in Fig. 2 , where the lowering of the temperature due to the excitation of resonances is shown (Hofmann,1976). If the number of resonances taken into account is increased, the temperature is substantially decreased compared to the calculation with a lower resonance number. This fact may also be viewed as the distribution of the internal energy over more degrees of freedom, which leads to a lower temperature. With the presently known experimental exponential increase of the hadronic mass spectrum, Hagedorn derived a limiting temperature for hadron-hadron collisions which is of the order of the pion rest mass

$$T^{Max} \approx m_\pi c^2 = 140 \text{ MeV} \quad . \tag{1}$$

However, according to fluid dynamical calculations one may read such a large temperature only for rather high bombarding energies, $E_{LAB} \gtrsim 10$ GeV/n. The best way to test whether a limiting temperature exists should be in a colliding beam experiment, with the much larger CM-energies available. One can convince oneself that a present CM-energies of the order of ✦ GeV/n, it may be difficult to decide experimentally whether the limiting temperature T^{Max} is reached, because of various concurting processes. One indication of a limiting temperature is that the pion production rate no longer increases, as the limiting temperature is reached. However, the decay of the known heavy resonances mainly produces pions, so $\langle n_\pi \rangle$ should nevertheless still increase.

Let us now consider another phenomenon, which may lead to a strong cooling of the nuclear system: According to Huber and Dilling(1978), the excitation energies of the isobaric resonances can be lowered coherently in a nuclear density, the so-called "Giant Isobaric Resonances", where

$$E^{GIR} - E_i^{\text{free } N^*} \approx 50 - 80 \text{ MeV} \; .$$

Such an effect, if it exists, may become even stronger in heavy ion reactions at

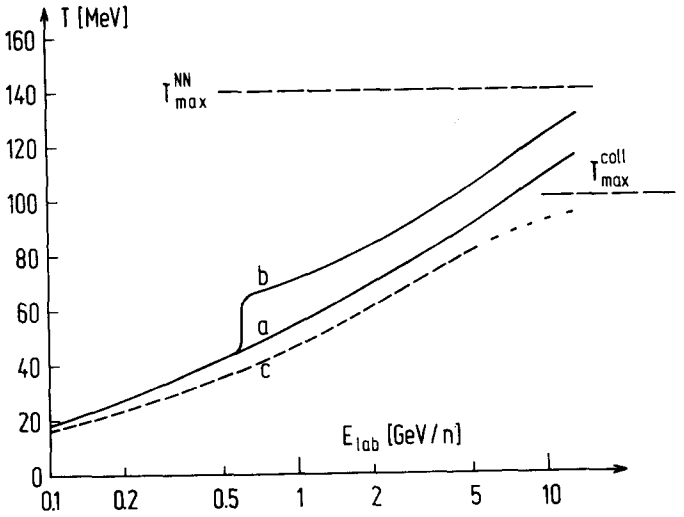

Fig.47. Shows the influence of the lowering of the resonance masses by 140 MeV each (dashed curve c)on the temperature. Curve b was obtained assuming a density isomer of depth -140 MeV.

high densities, and thus would lead to enhanced transformation of excitation energy into resonance masses, thus lowering the temperature of the system drastically (see Fig. 47). For an exponentially increasing hadronic mass spectrum a coherent lowering of the hadronic masses in the strongly interacting medium should lead to a collective limiting temperature T^{Max}, considerably lower ($T^{Max}_{coll} << T^{Max}_{NN}$) than for the free hadronic masses. Recently, however, it has been shown by different authors (Kapusta,1978; Weiner,1979) that the existence of a quark phase excludes an exponential raise of the hadron mass spectrum and therefore a limiting temperature. In fact there are experimental indications (Friedländer,1979) that there is no limiting temperature.

12. SPECULATIONS ON THE FORMATION OF EXOTIC NUCLEI

The high excitation energy per nucleon achievable in relativistic nuclear collisions may also serve as a tool for the production of exotic pieces of matter like e.g. A^{N*} nuclei, i.e. nuclei which include several nuclear resonances at once of even consist exclusively of nuclear resonances. This would allow the study of the many-particle interaction of N^* with each other. In close analogy, the formation of strange nuclei and even nuclei consisting of strange particles only may be feasible. A number of interesting problems concerning the mutual strange particle interaction have still to be solved. For very large energies, anti-nucleon production becomes feasible, where the total energy for baryon pair production as a collective process is large enough, while the energy per nucleon is still too small ("sub-threshold production"). These opportunities seem very speculative for the moment, however, some preliminary evidence for a strongly enhanced strange particle production process was recently discovered by Sandoval, Stock, Schroeder and coworkers (Sandoval,1979) in a streamer chamber experiment at Berkeley, where they found an order of magnitude increase of the Λ^0 production in RHI-collisions compared to pp-reactions. They measured the proportion $\langle m_{\Lambda^0}\rangle/\langle m_{\pi^-}\rangle$ for the system Ar→K at 1.8 GeV/n and found

$$\langle m_{\Lambda^0} \rangle / \langle m_{\pi^-} \rangle \sim 1.7\% \quad , \tag{1}$$

which is nearly an order of magnitude increase of the strange particle production compared to nucleon-nucleon collisions. This enhanced strange particle production is very exciting, as it points further to a collective production mechanism for heavy baryons. We can estimate the strange particle formation within the one-dimensional shock calculations as presented in section . The thermal excitation probability for a Λ^0 in this model is given by the product of the probability of Kaon production and Λ^0 production

$$\begin{aligned} p &\rightarrow \Lambda^0 + K^+ \\ n &\rightarrow \Lambda^0 + K^0 \end{aligned} \tag{2}$$

$$\frac{\langle m_{\Lambda^0}\rangle}{\langle m_n\rangle} \approx e^{-\frac{E_{\Lambda^0}}{T_s}} \cdot e^{-\frac{m_K c^2}{T_s}} \approx e^{-\frac{674\ \mathrm{MeV}}{T_s}} \quad . \tag{3}$$

The excitation function for Λ^0-production then looks similar to the π-production shown in Fig. 21 , however, with a much smaller value. Inserting the temperature T_s as obtained in the simple shock calculation into equation (3), we find

$$\langle m_{\Lambda^0} \rangle / \langle m_n \rangle \approx 0.0033. \tag{4}$$

Thus, from this rough estimate we obtain

$$\langle m_{\Lambda^0} \rangle / \langle m_{\pi^-} \rangle \approx 2.9\% \tag{5}$$

in reasonable agreement with the preliminary experimental result of Sandoval,Stock, Schroeder and co-workers (Sandoval,1979) and in fact an order of magnitude larger than what has been measured in pp-reactions.

13. SUMMARY AND OUTLOOK

We attempted to demonstrate that Relativistic Heavy Ion physics can open new fields in fundamental research. Very important is the unique opportunity to study the properties of nuclear (hadronic) matter under extreme conditions in fast nuclear collisions: We gave - in our view convincingly - circumstantial evidence for the existence of shock waves, i.e. various high compression and temperature effects in relativistic heavy ion collisions. The once promoted general transparency of nuclear matter at high energies does - as a general effect - not exist. It might only have validity as a quantum-fluctuation, which can, however, be separated experimentall from the strongly interacting nucleus-nucleus encounters. The high densities which may be achieved in relativistic collisions enable us to search for phase transitions (like pion condensation, density isomers) in nuclear matter and in particular for a transition of baryon into quark matter. These phase transitions themselves amplify because of critical scattering the validity of hydrodynamical and thermodynamical concepts. Therefore we can expect high compression effects to occur even up to bombarding energies of 10 GeV/n and higher. Also the experimental determination of the nuclear compression constant and sound velocity seems feasible. The high thermal excitations allow to study the successive transformation of nuclear matter into highly excited hadronic matter and the search for a limiting temperature. The collective formation of very heavy particles, bulks of strange matter and antimatter are further intriguing possibilities.

There are indications in the Mach-shock experiments of Schopper and Baumgardt (1979) that a phase transition of some kind (perhaps into a density isomeric configuration) might occur between 1.2 and 1.8 GeV/n. To check this out convincingly more refined experiments (excitation functions of α-particle angular distributions from multiplying events, pion production excitation functions) are necessary. Most important in this connection is also the further continuation of these experiments to higher energy up to e.g. 10 GeV/n and even higher energies.

REFERENCES

Anastasio, M.R., and G.E. Brown (1977). Nuc. Phys. A285, 516.
Antonenko, V.G., et al. (1979). Dubna preprint.
Baumgardt, H.G., J.U, Schott, Y. Sakamoto, E. Schopper, H. Stöcker, J. Hofmann, W. Scheid, and W. Greiner (1975), Z.Physik, A237,359.
Baym,G., and S.A. Chin (1976). Phys.Lett.,62B, 241.
Bertsch, G (1977). Phys.Rev.,C15,713.
Bodmer, A.R. (1971). Phys.Rev.,D4, 1601.
Brown, G.E., and W. Weise (1975). Phys.Rep., 22C, 279.
Brown, G.E., and W. Weise (1976). Phys.Rep., 27C, 1.
Buchwald, G. (1979). Thesis, University Frankfurt, unpublished.
Campbell, D.K., R.F. Dashen, J.T. Manassah (1975). Phys.Rev.,D12, 979 and 1010.
Chapline, G.F., M.H. Johnson, E.Teller, and M.S. Weiss (1973). Phys. Rev.,D8,4302.
Chodos, A., R.L. Jaffe, K. Johnson, C.B. Thorn, and V. Weisskopf (1974). Phys.Rev. D9, 3471.
Collins, J.C., and M.J. Perry (1975), Phys.Rev.Lett., 34, 1353.
Dalitz, R.H. (1976). Fundamentals of Quark Models, 17th Scottisch Universities Summer School in Physics, St. Andrews (ed. J.M. Barbour and A.T. Davis).
Ericson, T.E.O., and F. Myhrer (1978). Phys.Lett.,74B, 163.
Feenberg, E., and H. Primakoff (1946). Phys.Rev.,70, 980.
Fowler, G.N. and R.M. Weiner (1979). To be published.

Freedman, B., and L.McLerran (1978). Phys.Rev., D17, 1109.
Friedländer, E. (1979). Private communication.
Fung, S.Y., W. Gorn, G.P. Kiernan, J.J. Lu, Y.T. Oh, and R.T. Poe (1978), Phys.Rev. Lett., 41, 1592.
Galitskii, V.M., and I.N. Mishustin (1978). Phys.Lett., 72B, 285.
Greiner, W. (1975). Talk at the 3rd High Energy Heavy Ion Summer Study, Berkeley, Calif.
Gyulassy, M., and W. Greiner (1977). Ann.Phys., 109, 485.
Hagedorn, R. (1965). Supp. Nuovo Cim., III, 2, 147.
Heinz, U., H. Stöcker, and W. Greiner (1978). Proc. Symp. on Relativistic Heavy Ion Research, GSI, Darmstadt.
Hofmann, J., H. Stöcker, W. Scheid, and W. Greiner (1974). Rep. of the Workshop on BEV/Nucleon Collisions of Heavy Ions, Bear Mountain, New York.
Hofmann, J., W. Scheid, and W. Greiner (1976). Nuovo Cim., 33A, 343.
Hofmann. J., H. Stöcker, M. Gyulassy, W. Scheid, and W. Greiner (1976). Proc. Int. Conf. on Selected Topics in Nuclear Structure, Dubna (USSR)
Hofmann, J., H. Stöcker, U. Heinz, W. Scheid, W. Greiner (1976). Phys.Rev.Lett.,36, 88.
Hofmann, J., B. Müller, and W. Greiner (1979). Phys. Lett., 82B, 195.
Irvine, J.M. (1975). Rep. Prog. Phys., 38, 1385.
Kapusta, J.I. (1979). Nuc. Phys., B148, 461.
Keister, B.D., and L.S. Kisslinger (1976). Phys. Lett., 64B, 117.
Kisslinger, L.S. (1955). Phys. Rev., 98, 761.
Lee, T.D., G.C. Wick (1974). Phys.Rev., D9, 2291.
Maruhn, J.A. (1977). Proc. Conf. on Heavy Ion Collisions, Oak Ridge, Tenn., p.156.
Mattuck, R.D., and B. Johansson (1968). Adv. Physics, 17, 509.
Meyer, W., H. Gutbrod, R. Stock, A. Poskanzer, A. Sandoval, et al. (1978). To be published.
Migdal, A.B. (1967). Theory of Finite Fermi Systems and Applications to Atomic Nuclei. Interscience, New York.
Migdal, A.B. (1972). JETP, 34, 1184.
Migdal, A.B. (1978) Rev. Mod. Phys., 50, 107.
Nagamiya, S., et al. (1979). Phys.Lett., 81B, 147.
Ne'eman, Y. (1974). Physics of Dense Matter (ed. C.J. Hansen), Reidel, Dordrecht, Boston, p. 111.
Richardson, J.L. (1979). Phys. Lett., 82B, 272.
Ruck, V., M. Gyulassy, and W. Greiner (1976). Z. Physik, A277,391.
Sandoval, A., R. Stock, L. Schroeder, et al. (1979). To be published.
Sawyer, R.F., and D.J. Scalapino (1973). Phys. Rev. D7, 953.
Scheid, W., R. Ligensa, and W. Greiner (1968). Phys. Rev. Lett., 21, 1479.
Scheid, W., and W. Greiner (1969). Z.Physik, 226, 365.
Scheid, W., H. Müller, and W. Greiner (1974). Phys. Rev. Lett., 32, 741.
Scheid, W., J. Hofmann, and W. Greiner (1974a). Proc. of the 2nd High Energy Heavy Ion Summer Study, Berkeley, Calif. (ed. L.S. Schroeder), LBL Report No. LBL-3675.
Schopper, E. and H.G. Baumgardt (1979). Priv. communication.
Sobel, M.I., P.J. Siemens, J.P. Bondorf, and H.A. Bethe (1975). Nuc.Phys. A251, 502.
Stanley, H.E. (1971). Introduction to Phase Transitions and Critical Phenomena, Clarendon Press, Oxford.
Stöcker, H., W. Scheid, and W. Greiner (1977). Proc. of the Topical Conf. on Heavy Ion Collisions, Fall Creek Falls State Park, Oak Ridge, USA.
Stöcker, H., J. Hofmann, W. Scheid, and W. Greiner (1977a). Conf. on Nuclear Collisions, Bled, Yugoslavia. Fizika 9, Supp. 4, 671.
Stöcker, H. W. Greiner, and W. Scheid (1978). Z.Physik, A286, 121.
Stöcker, H., J. Reinhardt, J.A. Maruhn, and W. Greiner (1978a). Proc. Workshops on Heavy Ion Physics, Saclay (France).
Stöcker, H., J.A. Maruhn, and W. Greiner (1979). Z. Physik, A290, 297.
Stöcker, H., J.A. Maruhn, and W. Greiner (1979a). Phys. Rep. To be published.
Stöcker, H., J.A. Maruhn, and W. Greiner (1979b). Phys. Lett., 81B, 303.

Stöcker, J.A. Maruhn, and W. Greiner (1979c). To be published.
Vasak, D., B. Müller, and W. Greiner (1979). To be published.
Weise, W., and P. Hecking (1979). To be published.
Wolf, K.L. et al. (1979). Phys. Rev. Lett., 42, 1448.
Wong, C.Y., and T.A. Welton (1974). Phys. Lett., 49B, 243.
Wong, C.Y., J.A. Maruhn, and T.A. Welton (1977). Phys. Lett., 66B, 19.

Kurzbiographie

Horst Stöcker
geb. 16. Dezember 1952 in Frankfurt am Main
Privatadresse:
Grabenstrasse 5
6370 Oberursel 5

Ausbildung:

1959 - 1963	Grundschule Weißkirchen am Taunus
1963 - 1971	Gymnasium Oberursel
1971	Abitur
1971 - 1976	Studium der Physik, Mathematik und Chemie an der Johann Wolfgang Goethe Universität Frankfurt am Main
1976	Physik-Diplom unter Leitung von Herrn Prof. Dr. Walter Greiner Titel der Diplomarbeit: "Nukleare Schockwellen und Machschockkegel in relativistischen Schwerionenstössen" Note: sehr gut
1976 - 1979	Assistent am Institut für theoretische Physik der J.W. Goethe Universität Frankfurt am Main
Frühjahr 1978	Forschungsaufenthalt am Oak Ridge National Laboratory, Oak Ridge, Tennessee und an der Vanderbilt University, Nashville, Tennessee
seit Juli 1979	Gastwissenschaftler bei der Gesellschaft für Schwerionenforschung (GSI), Darmstadt